Available online at www.sciencedirect.com
SCIENCE DIRECT
Geochimica et Cosmochimica Acta 70 (2006) 3096–3120
Geochimica
www.elsevier.com/locate/gca

Evidence from Antarctic mantle peridotite xenoliths for changes in mineralogy, geochemistry and geothermal gradients beneath a developing rift

S.F. Foley [a,*], A.V. Andronikov [b], D.E. Jacob [a], S. Melzer [c,d]

[a] *Institut of Geosciences, University of Mainz, Becherweg 21, 55099 Mainz, Germany*
[b] *Department of Geological Sciences, University of Michigan, Ann Arbor, Michigan, USA*
[c] *GeoForschungsZentrum Potsdam, Postfach 600751, D-14407, Potsdam, Germany*
[d] *Ceramics Research Centre, Corus RD & T, Addresscode 3J22, 1970 CA IJmuiden, The Netherlands*

Received 3 January 2006; accepted in revised form 23 March 2006

Abstract

Garnet and spinel peridotite xenoliths associated with the Phanerozoic Lambert–Amery Rift in eastern Antarctica contain evidence for several stages in the development of the mantle beneath the rift. Despite the fact that equilibria were only partly attained, a combination of petrography, whole-rock geochemistry, mineral chemistry and thermobarometry can be used to decipher four stages prior to entrainment of the xenoliths in the host magma during the initial stages of the breakup of Antarctica, India and Madagascar. The first chronological stage is represented by harzburgitic protoliths represented by rare occurrences of low-Ca olivines and orthopyroxenes in spinel lherzolites: these yield the lowest temperatures of 830–850 °C, and are also characterized by distinct trace element contents; lower Ti, Cr, V and Zn in olivine and orthopyroxene, and additionally lower Cu, Ni, Ga and Li in orthopyroxene. Some garnets are subcalcic, indicating that the spinel–garnet lherzolites also formed from harzburgitic protoliths. The second stage is the formation of garnet due to a pressure increase probably related to collision at 1.1 Ga. The third stage is marked by the growth of clinopyroxene, demonstrably in cpx-poor spinel lherzolites but probably in all xenolith groups: equilibrium of clinopyroxene with olivine and orthopyroxene was not attained in all samples, so that the non-judicious use of thermobarometers can produce bewildering results. The fourth stage is an enrichment episode that affected all spinel–garnet peridotites and about half of the spinel peridotites. During this stage, reaction rims were produced on the clinopyroxenes that formed during stage 3, the modal content of olivine and Mg/(Mg + Fe) in the rocks was reduced, CaO, Al_2O_3 and trace elements were enriched, and garnets were almost completely transformed to kelyphites. A later stage is documented by interstitial glasses and films around spinels related to infiltration of melt from the host magma. These post-date, and are more enriched in alkalies than, partially melted rims on clinopyroxenes, demonstrating that all the three earlier episodes were pre-entrainment events. Pressures indicated by the spinel + garnet lherzolites are restricted to 20–24 kbar at 1040–1180 °C. Early harzburgitic assemblages are interpreted to represent an earlier, cooler geotherm, whereas the kelyphite assemblages indicate temperatures 180–200 °C hotter than the main xenolith geotherm. This event also caused recrystallization of the clinopyroxene rims and is attributed to heating during rifting, but not due to the host magma itself. The preservation of evidence for three progressively hotter geotherms can be related to the upward movement of isotherms during the development of the sub-rift mantle.

1. Introduction

Rifting of continental crust is accompanied by a progression from colder thicker lithosphere to warmer thinner lithosphere, irrespective of whether the role of the underlying mantle in rifting is passive or active. Rifts vary

* Corresponding author. Fax: +49 6131 39 23070.
E-mail address: foley@uni-mainz.de (S.F. Foley).

0016-7037/$ - see front matter © 2006 Elsevier Inc. All rights reserved.
doi:10.1016/j.gca.2006.03.010

from prominent examples in which crust and lithosphere are merely thinned, such as the East African (Mechie et al., 1997) or Rio Grande Rifts (Wilson et al., 2005) to extreme examples where a former craton has been split and rifting has proceeded to the production of oceanic crust, such as in the Labrador Sea (Chalmers and Laursen, 1995).

Although the development of the sub-rift mantle is frequently mapped out by geophysical means, little is known first-hand about its changing petrology and composition through studies of mantle xenoliths. Much effort has been expended in describing the characteristics and differences between cratonic and non-cratonic xenoliths (Harte, 1983; Menzies, 1983), in the recognition of enrichment processes and their effects, and in the delineation of fossil geotherms in various regions, but relatively little on rift related processes as recorded in xenoliths.

In the Jetty Peninsula area of eastern Antarctica there is a little known occurrence of garnet–spinel–lherzolite xenoliths, the only such suite reported in Antarctica (Grikurov et al., 1980; Andronikov, 1990). In addition to offering a rare opportunity to study the mantle beneath Antarctica, they have further value in providing insight into an area where a stable craton was split by a major continental rift during the separation of India from eastern Antarctica. In this respect, the Jetty Peninsula xenoliths have well-studied counterparts in only two areas, the central East African rift, in which a variety of ultramafic xenoliths including garnet-bearing lherzolites have been described (Rhodes and Dawson, 1975; Henjes-Kunst and Altherr, 1992; Rudnick et al., 1994), and the Vitim plateau in Siberia, in which garnet-spinel lherzolites may be distally related to the Baikal Rift (Ionov et al., 1993; Glaser et al., 1999). Alkaline intrusives related to the Labrador Sea rift, which split the North Atlantic craton, are also known to contain garnet lherzolites (Emeleus and Andrews, 1975; Andrews and Emeleus, 1976; Bizzarro and Stevenson, 2003).

Although common in the xenolith suites of kimberlites and related rocks from all continents (Harte, 1983; Boyd and Mertzmann, 1987; Boyd et al., 1997), garnet- and garnet + spinel lherzolite xenoliths occur only rarely in non-kimberlitic rocks outside cratonic regions. Well-studied examples are known from Pali-Aike close to the Chile-Argentina border (Skewes and Stern, 1979; Stern et al., 1989; Kempton et al., 1999a,b), from the Navajo volcanic field in Arizona/New Mexico (Ehrenberg, 1982), to the east and south of Lake Baikal in eastern Siberia (Ionov et al., 1993; Ashchepkov et al., 1994; Glaser et al., 1999; Litasov et al., 2000), from eastern China (Fan and Hooper, 1989; Qi et al., 1995; Xu et al., 1998), and from Malaita, Solomon Islands (Nixon and Coleman, 1978; Delaney et al., 1979). These occurrences are important as representatives of the deepest samples of the mantle from non-cratonic regions, and, due to the presence of garnet, can be used to estimate the pressure and temperature of origin of the xenoliths with much more certainty than is possible for garnet-free spinel lherzolite xenoliths.

In this paper, we present the main petrological and mineral chemical features of the peridotite xenolith suite from the Jetty Peninsula, and show that the features they contain can be interpreted in terms of long-term events in the lithospheric mantle, particularly thermal events during the development of a major rift.

2. Geological setting

The Jetty Peninsula is located at the edge of the Amery ice shelf on the flank of the Beaver Lake rift system which was generated at about 650 Ma and lies nearly parallel to, and on the western side of, the larger Lambert–Amery Rift which developed during Mesozoic–Cenozoic times (Kurinin and Grikurov, 1980; Andronikov and Beliatsky, 1995). The Lambert–Amery Rift dominates the regional geology and structure and stretches more than 700 km inland from the coast, cutting through all known Proterozoic and Archean basement rock groups of the region (Fig. 1). The Prince Charles Mountains of MacRobertson Land (Fig. 1) represent the best exposed section of the Precambrian East Antarctic Shield (Ravich et al., 1984; Sheraton et al., 1996), although exposure is very limited by the continental ice. There are few modern geochronological data for Archaean rocks of the southern Prince Charles Mountains; Rb-Sr isochron ages of granitic gneisses are about

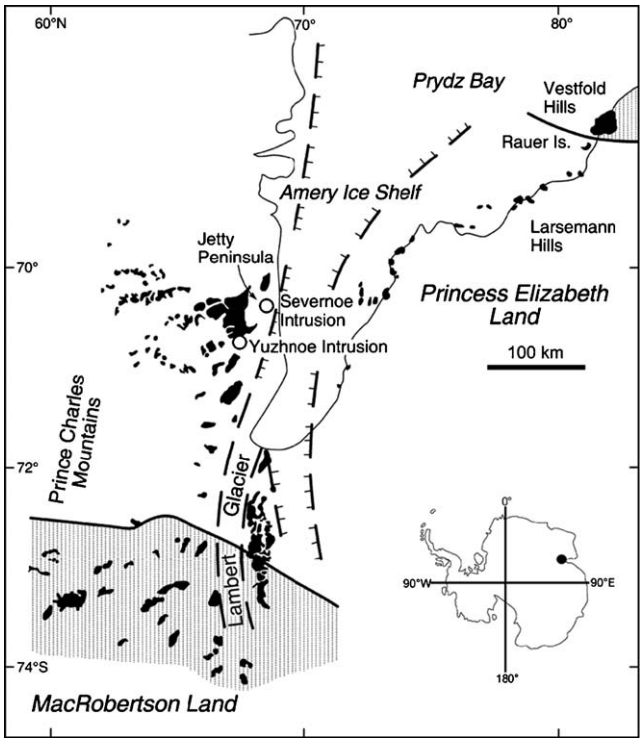

Fig. 1. Schematic map of the Lambert-Amery Rift area (after Tingey, 1991 with additions). Outcrops are shown in black, the coastline with a thin solid line, and the position of the Lambert-Amery Rift with hatched lines. The shaded area is known to be underlain by Archean rocks of the east Antarctic craton. The xenoliths are from the Yuzhnoe (southern) intrusion.

2700–2800 Ma (Tingey, 1991), and there are a few somewhat older U–Pb zircon ages at 3000–3200 Ma (Kovach and Beliatsky, 1991).

Mantle xenoliths are also known in Proterozoic (1.3–1.7 Ga) ultramafic lamprophyres which cut the Archaean high-grade metamorphic terrane of the Vestfold Hills further to the northeast (Fig. 1; Andronikov et al., 1994; Andronikov and Mikhalsky, 1997). Thus, although located relatively close to the Lambert–Amery Rift where the Jetty Peninsula xenoliths occur, they were sampled much earlier and are unrelated in terms of the mantle lithospheric events they have experienced. The mantle xenoliths of Jetty Peninsula occur in a series of Mesozoic (140–150 Ma; Laiba et al., 1987) alkaline ultramafic rocks. Xenoliths have been found in two intrusive bodies (Fig. 1). Xenoliths from these two bodies differ markedly in terms of petrography and mineralogy; about 90% of xenoliths from the southern body are lherzolites, including garnet-bearing varieties, with subordinate harzburgite and dunite. In contrast, xenoliths from the northern intrusion comprise harzburgite (50%), garnet-free lherzolite (25%), and subordinate wehrlite and dunite, and appear to be derived from higher levels in the mantle.

3. The southern intrusion and its xenolith types

The southern intrusion consists of a dyke-like body 150 m long and up to 20 m wide, with a subcircular eastern end 80–85 m in diameter. Two intrusive episodes can be recognized: the first occurs in the northern part of the body and is characterized by an alkali-picritic breccia rich in highly carbonated lapilli; the second phase makes up most of the intrusion and is composed of phlogopite- and pyroxene-bearing alkali-picrites (Andronikov, 1990; Andronikov and Egorov, 1993). Mantle-derived xenoliths comprise up to 30% of the rock volume. The chemical composition of the alkali-picrites is given in Table 1: the occurrence of the xenoliths in these rocks is interesting, as spinel–garnet lherzolite xenoliths are carried by alkali picrites in the Vitim plateau in Siberia (Litasov et al., 2000), and by ultramafic lamprophyres on the borders of the Labrador Sea (Tappe et al., 2006). The Antarctic alnöites have very high MgO contents and Mg# (100Mg/(Mg + Fe)) and extremely high volatile contents (CO_2 contents up to 9.6 wt%). CaO contents are much lower than in ultramafic lamprophyres of olivine–melilititic affinity which occur close by because of the dominance of olivine and phlogopite (Andronikov, 1990; Foley et al., 2002). The rocks are richer in MgO than the alkali picrites in Siberia.

Table 1
Representative chemical analyses of the host alkali picrites

SiO_2	39.1	35.6
TiO_2	1.48	1.74
Al_2O_3	6.53	5.76
Fe_2O_3	0.96	1.51
FeO	6.52	6.86
MnO	0.15	0.17
MgO	18.1	23.8
CaO	8.08	9.10
Na_2O	1.42	1.48
K_2O	1.80	1.74
P_2O_5	0.60	0.66
LOI	15.06	11.86
Total	99.88	100.24
CO_2	9.57	8.16
Mg#	81.4	83.7
FeO total	7.38	8.22

The majority of the xenoliths are ovoid in shape and range in size from 5 to 30 cm, locally reaching 50 cm in diameter (Andronikov, 1990). Three main groups of lherzolites can be identified on the basis of mineral assemblage, textural relationships between the minerals, and mineral composition; (i) cpx-poor spinel lherzolites, (ii) cpx-rich spinel herzolites, and (iii) garnet + spinel lherzolites.

3.1. Clinopyroxene-poor spinel lherzolites (CPSL)

Cpx-poor spinel lherzolites show no pronounced textural evidence of reaction relationship between mineral phases and have homogeneous mineral major element compositions. Crystals are medium to coarse grained, inequigranular and can have well-developed triple-point junctions. Olivine and clinopyroxene crystals are up to 2–3 mm across; orthopyroxenes are generally smaller (0.3–0.7 mm), whereas spinels form either small (<0.1 mm) red-brown equigranular crystals or large (up to 1–1.5 mm) amoeboid grains (Fig. 2a). Large spinel grains may contain small (<0.1 mm) olivine inclusions, and inclusions of olivine and orthopyroxene occur within larger orthopyroxene and olivine grains. Texturally identifiable products of intra-mantle metasomatic reaction are extremely rare in this group: minor glass occurs as thin films (15–20 μm) around spinel grains, and small (<0.01 mm) oval carbonate blebs can be distinguished between pyroxene grains. Modal mineral composition of the xenoliths determined by point counting are given in Table 2. These show higher modal olivine and lower modal clinopyroxene for the CPSL than for the other two groups; clinopyroxene averages only 5% modally in contrast to >11% in the other two groups.

3.2. Clinopyroxene-rich spinel lherzolites (CRSL)

Cpx-rich spinel lherzolites show abundant evidence for reaction relationships between minerals. Mineral compositions are typically inhomogeneous and may be strongly zoned from core to rim. Textures are coarse inequigranular with the size of olivine, pyroxenes and spinel generally ranging between 0.5 and 1.0 mm (Fig. 2b). Large orthopyroxene grains (up to 2–3 mm) are uncommon. Small grains of olivine and spinel (0.1–0.2 mm) may be

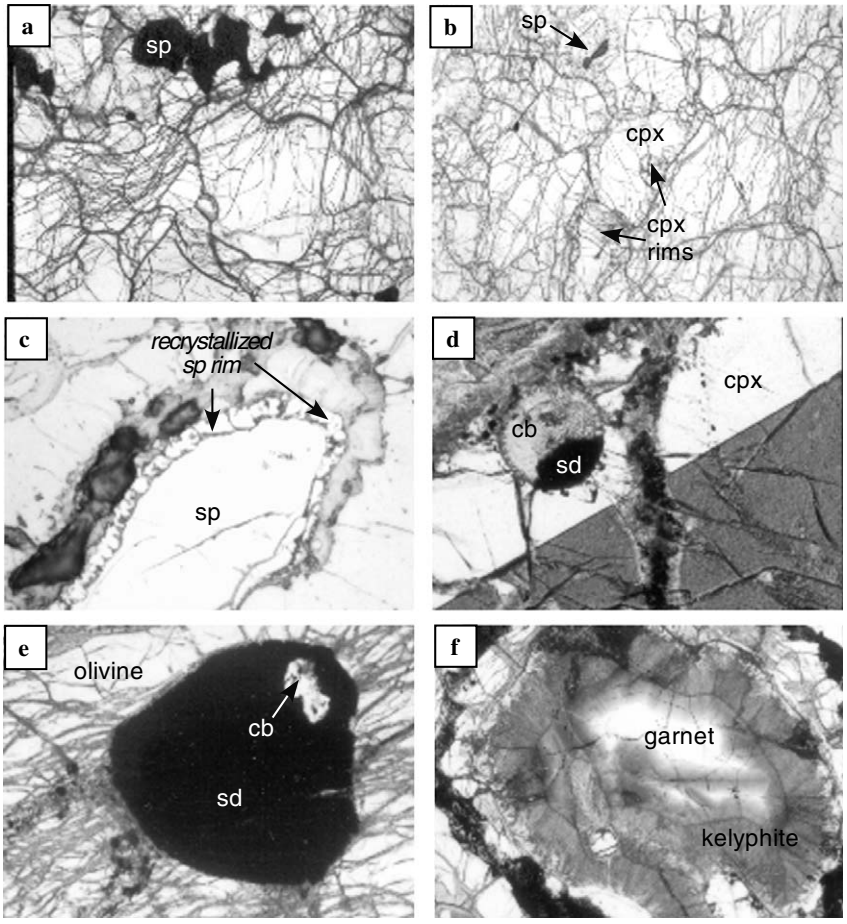

Fig. 2. Photomicrographs of Jetty Peninsula lherzolite xenoliths. (a) Clinopyroxene-poor spinel lherzolite showing irregular form of spinels (photo width 6 mm); (b) Clinopyroxene-rich spinel lherzolite showing recrystallization of clinoypyroxene rims (photo width 6 mm); (c) Reflected light photo (width 0.7 mm) of recrystallized rim of spinel. These reaction rims contain glass interpreted to result from melts largely of external origin; (d) Rounded bleb of carbonate (cb) > sulphide (sd) enclosed in clinopyroxene (photo width 0.7 mm); (e) Rounded sulphide mineral with small inclusion of carbonate, itself included in olivine (photo width 0.7 mm); (f) Kelyphite mantle around garnet (photo width 6 mm). Most examples are more thoroughly altered to kelyphite than this.

included in larger orthopyroxene and olivine crystals. Kink-bands in olivine and orthopyroxene show a greater degree of deformation than observed in CPSL. Late metasomatic and/or incipient melting events are evident as recrystallized rims of clinopyroxene (Fig. 2b) and more rarely spinel (Fig. 2c). These rims may replace as much as 90% of the original minerals. The recrystallized clinopyroxene has a spongy appearance in thin section due to numerous micrometre-sized glass inclusions. Further indications for the chemical nature of the metasomatic agent are given by small (<10 μm) carbonate + sulphide blebs occurring as inclusions in silicate minerals (Fig. 2d), and carbonate inclusions in sulphides (Fig. 2e). These chemical characteristics show that the recrystallization of clinopyroxenes to form the spongy rims was accompanied by minor infiltration of material. The modal abundance of clinopyroxene is higher (9–14%) and that of olivine lower (66–75% vs. 78–82%) than in cpx-poor spinel lherzolites, whereas the abundances of orthopyroxene and spinel are similar in both groups (Table 2).

3.3. Spinel–garnet Lherzolites (SGL)

The spinel–garnet lherzolite group shares many of the textural features of the clinopyroxene-rich spinel lherzolites, but differs by the presence of garnet (Fig. 2f), most of which is totally transformed to kelyphite. The texture is coarse inequigranular, partly porphyroclastic because of the presence of kelyphite aggregates after garnets that are up to 3 cm in diameter. The average grain size of the other silicate minerals is 0.5–0.8 mm although single olivine grains may be up to 4 mm in diameter. Spinel is relatively rare (<1%) and can be present either as nearly idiomorphic or as amoeboid interstitial grains. Kink-bands in primary olivine and orthopyroxene are common. Evidence for metasomatic infiltration or incipient melting is similar to the CRSL in the development of reaction rims around clinopyroxene and spinel, but these rims are thinner than in the CRSL. Another feature of the SGL is the sporadic development of small clinopyroxene and olivine neoblasts adjacent to primary orthopyroxene grains. Thin (10–30 μm) intergranular films of glass may be developed between various

Table 2
Modal mineralogy of lherzolite xenoliths from the Jetty Peninsula

Sample	Ol	Opx	Cpx	Ga	Spl	Sulf	Carb
Cpx-poor spinel lherzolites (CPSL)							
U-3	80	13	4.5		2.5	+	+
D-11	82	12.5	3.5		1.5	+	
U-3/4-2	78.5	12	6.5		3	+	
D-24	78	14	4.5		3.5	+	+
D-N2	82	11	4		3		
1/4-3	79	12.5	5		3.5	+	+
32601-9B	78	10	7		5	+	
Average	79.6	12.1	5.0	0.0	3.1		
Cpx-rich spinel lherzolites (CRSL)							
U-1	69	16	14		1		+
U-4/9-2	75	11	9		4	+	+
U-36*	66	16	11		2		+
U-N1	72	14	12		2	+	+
XLT-4	71	14	12		3		+
XLT-5	70	15	12		3	+	+
Average	70.5	14.3	11.7	0.0	2.5		
Spinel–garnet lherzolites (SGL)							
U-3/3A	58	22.5	16.5	2.5	0.5		+
U-16	60	22	14	3.7	0.3		+
U-17	66	18.5	13	2	0.5		+
U-47	60.5	22	12	5	0.5		+
D-A3	68	19	11	1.5	0.5		+
DK-8/3	62	21.5	12	4	0.5		+
D-N1	63.5	19.5	13	3.8	0.2	+	+
D-N4	62	19	13.5	5	0.5	+	+
3/1-3	66.5	18	12	3	0.5	+	+
15/1-2	57	21	15	6.8	0.2		+
XLT-1	61	20.6	15	3	0.4		+
Average	62.2	20.3	13.4	3.7	0.4		

Mineral modes given in vol%. Presence of trace sulphides and carbonates (<1%) denoted by +. *, Sample U-36 additionally contains 5% glass patches.
Abbreviations: Ol, olivine; Opx, orthopyroxene; Cpx, clinopyroxene; Ga, garnet; Spl, spinel; Sulf, sulphides and Carb, carbonates.
Values given for garnet include volumes now occupied by kelyphite.

silicate mineral grains. Large olivine grains may contain inclusions of smaller olivines and orthopyroxenes and very rarely small blebs of carbonate. The SGL group appears to represent higher pressure equivalents of the CRSL group, differing essentially only in the presence of garnet, whereas no unmetasomatized garnet-bearing equivalents of the CPSL group have been found. The modal abundance of olivine is lower and that of orthopyroxene higher in SGL than in CRSL (Table 2).

4. Geochemistry of Jetty Peninsula peridotite xenoliths

Table 3 presents XRF whole-rock compositions for all peridotite samples studied. The Jetty Peninsula xenoliths have Mg# 87–91.6, similar to mantle peridotites from non-cratonic continental occurrences worldwide (Frey and Prinz, 1978; Menzies, 1983; Preß et al., 1986; Henjes-Kunst and Altherr, 1992; Vaselli et al., 1995). On a plot of Mg# of olivine against modal olivine content (Fig. 3), they fall along the oceanic depletion trend of Boyd (1989) in a generally similar position to garnet + spinel peridotites from the Vitim area (Ionov et al., 1993; Glaser et al., 1999) and Pali Aike (Kempton et al., 1999a). They are distinct from the low temperature cratonic peridotites of Kaapvaal and Siberia, which lie to higher Mg# for a given modal olivine content (Boyd and Mertzmann, 1987; Boyd et al., 1997), and also from the exceptionally depleted West Greenland harzburgites (Bernstein et al., 1998). Fig. 3 shows that the Jetty Peninsula clinopyroxene-poor spinel lherzolites have higher modal olivine contents and are distinctly and uniformly more depleted than the SGL and CRSL groups, and that the CRSL show more scatter away from the depletion trend towards lower Mg#. The more depleted character of the CPSL is also apparent from plots of Mg# against CaO and Al_2O_3 of the whole rocks (Fig. 4). The peridotites of Vitim and Pali Aike are similar to undepleted mantle (Mg# 89.3, CaO = 3.54 wt%, Al_2O_3 = 4.44 wt%; McDonough and Sun, 1995), and offset to higher CaO and Al_2O_3 relative to rocks from the other localities shown in Fig. 4. The Jetty peninsula SGL are similar to Vitim and Pali Aike in CaO contents, whereas they plot to somewhat lower contents of Al_2O_3. The CRSL again show more scatter, but are more similar to the SGL than the depleted CPSL. It thus appears from the whole-rock compositions that the clinopyroxene-rich spinel lherzolites and garnet + spinel lherzolites have more prim-

Table 3
Major element composition of Jetty Peninsula lherzolite xenoliths

Rock group	Cpx-poor spinel lherzolites						Cpx-rich spinel lherzolites					Spinel–garnet lherzolites								
Sample	U-3	D-11	U-3/4-2	D-24	D-N2	1/4-3	32601-9B	U-1	U-4/9-2	U-36	U-N1	XLT-4	XLT-5	U-3/3A	U-16	U-17	U-47	D-A3	DK-8/3	D-N1	D-N4	3/1-3	15/1-2	XLT-1
SiO_2	42.0	42.0	40.7	42.0	41.2	40.9	41.9	43.4	43.9	41.5	41.4	40.6	41.3	41.5	43.4	43.3	42.8	42.6	41.7	42.2	43.2	43.1	39.1	43.3
TiO_2	0.04	0.01	0.07	0.01	0.02	0.01	0.01	0.13	0.04	0.13	0.13	0.30	0.09	0.14	0.07	0.15	0.07	0.10	0.08	0.12	0.16	0.09	0.46	0.18
Al_2O_3	1.20	1.14	0.53	1.18	1.17	1.30	1.63	3.00	1.99	2.57	2.40	2.19	3.02	3.20	4.10	2.33	2.60	3.00	2.80	2.82	3.00	2.98	3.00	2.45
Cr_2O_3	0.45	0.46	0.26	0.54	0.66	0.70	0.57	0.37	0.31	0.21	0.34	0.37	0.19	0.27	0.24	0.12	0.36	0.39	0.41	0.21	0.25	0.29	0.28	0.20
FeO	8.41	7.84	8.47	7.88	8.00	7.9	7.47	7.99	6.94	7.79	7.74	9.06	7.44	7.85	7.57	8.09	7.42	8.20	7.98	8.19	8.14	8.57	7.83	8.66
MnO	0.12	0.18	0.12	0.18	0.17	0.15	0.24	0.09	0.11	0.15	0.12	0.13	0.12	0.12	0.15	0.19	0.13	0.13	0.13	0.17	0.15	0.17	0.12	0.13
MgO	44.2	44.7	44.8	44.7	45.3	45.4	44.6	37.6	40.1	39.9	38.9	41.0	39.5	38.9	38.0	39.0	38.2	40.5	38.9	39.5	38.8	39.1	34.5	37.8
CaO	0.90	0.98	0.84	1.14	1.03	1.01	1.50	2.75	1.96	2.41	2.20	2.01	3.34	2.75	3.35	2.87	2.50	2.40	2.30	3.01	2.89	2.85	2.39	2.65
Na_2O	0.10	0.03	0.11	0.04	0.05	0.05	0.04	0.25	0.09	0.25	0.20	0.12	0.22	0.25	0.19	0.19	0.20	0.40	0.10	0.22	0.19	0.18	0.52	0.16
K_2O	n.d.	n.d.	0.11	n.d.	0.01	0.01	n.d.	0.05	0.03	0.11	0.10	0.15	0.01	0.04	0.04	0.02	n.d.	n.d.	n.d.	n.d.	n.d.	0.04	0.44	0.08
P_2O_5	0.02	0.01	0.04	0.02	0.01	0.02	0.01	0.03	0.04	n.d.	0.03	0.01	n.d.	0.03	0.01	0.02	0.03	0.02	0.03	n.d.	n.d.	0.02	0.23	0.03
LOI	1.60	2.04	3.44	2.19	1.52	2.07	2.01	4.63	3.41	4.53	5.30	3.67	3.64	5.35	1.75	4.04	5.40	2.85	5.50	3.41	3.15	3.18	10.07	4.03
Total	99.26	99.52	99.67	100.10	99.31	99.76	100.11	100.51	99.12	99.77	99.04	99.91	99.05	100.59	99.51	100.46	99.87	100.82	100.49	100.02	100.09	100.70	99.18	99.81
Mg#	91.2	90.4	90.9	90.9	90.7	90.8	90.2	89.5	87.7	86.8	90.9	89.0	89.6	91.2	89.9	90.0	88.8	90.8	89.8	89.1	89.0	89.9	89.6	89.6

Mg# = 100 * Mg/(Mg + Fe).

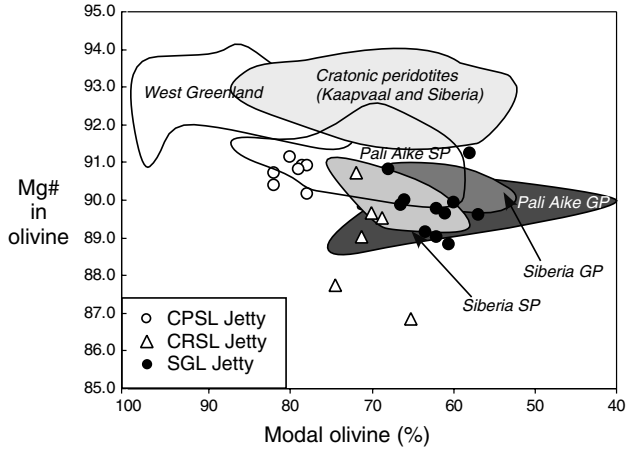

Fig. 3. Mg# of olivine vs. modal olivine content for Jetty Peninsula lherzolites compared to other spinel + garnet lherzolite localities of Pali Aike, Chile (unshaded and darkest shading; Kempton et al., 1999a,b) and Vitim, Siberia (two shadings for garnet (GP) and spinel (SP) peridotites; Ionov et al., 1993; Glaser et al., 1999). The Jetty Peninsula samples lie on the oceanic trend of Boyd (1989) and are distinct from Kaapvaal and Siberia cratonic peridotites, which have higher Mg# olivines for a given modal olivine content. Jetty Peninsula clinopyroxene-poor spinel lherzolites (CPSL) have higher modal olivine than clinopyroxene-rich spinel lherzolites (CRSL) and spinel + garnet lherzolites (SGL). The CRSL show more scatter to lower Mg#. Other data sources: Kaapvaal peridotites from Boyd and Mertzmann (1987), West Greenland from Bernstein et al. (1998).

itive compositions than the clinopyroxene-poor spinel lherzolites, although it remains to be ascertained to what proportion the composition of all rock types is influenced by re-enrichment of protoliths by melt infiltration. The higher P_2O_5 contents in some xenoliths indicate a higher degree of infiltration by the host melt and not to the presence of modal apatite as known from other peridotites (Chazot et al., 1996a,b).

5. Major element compositions of minerals

Major element compositions of xenolith minerals were analysed by a CAMECA SX 50 microprobe at University of Tasmania (Hobart, Australia), and by a CAMECA SX 100 microprobe at GeoForschungsZentrum (Potsdam, Germany), with an accelerating voltage of 15 kV and a beam current of 20 nA. Where grain sizes permitted, a wide diameter electron beam (10–20 μm) was used to prevent strong alkali volatilization, especially for analysis of glass compositions. The main chemical parameters for representative primary minerals of each sample are summarized in Table 4, and analyses are given for mineral rims, neoblasts, and the components of kelyphitic rims around garnets in Table 5.

5.1. Olivine

Olivines from all three groups of Jetty Peninsula peridotites are relatively uniform in composition and characteristic of fertile to moderately depleted rock compositions (89.3–91.8). Olivines in the CPSL appear to be uniform;

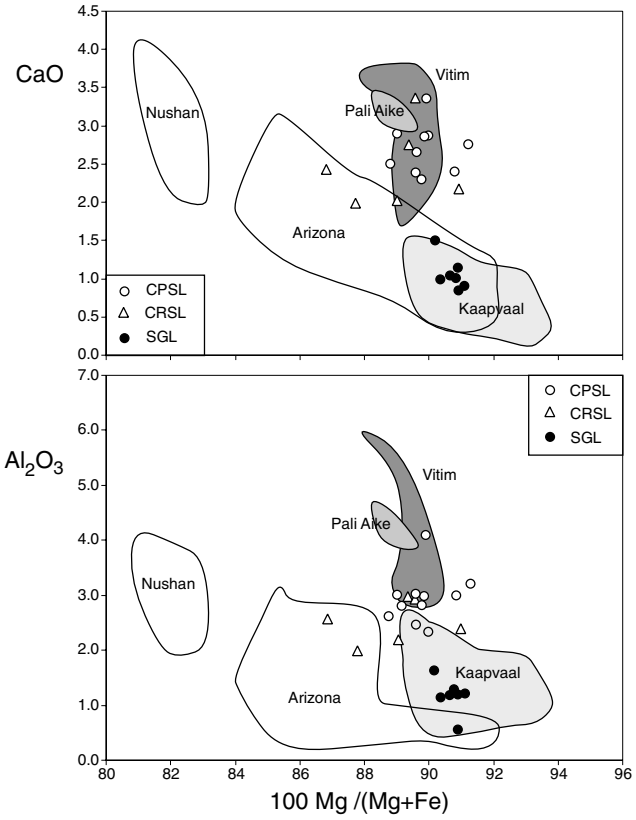

Fig. 4. Mg# of whole-rocks vs. CaO and Al_2O_3 indicates more depleted character of Jetty Peninsula spinel lherzolites relative to clinopyroxene-rich spinel lherzolites (CRSL) and spinel + garnet lherzolites (SGL). Mantle depletion by basalt loss is represented by the trend from Nushan peridotites (Xu et al., 1998) through Arizona (Ehrenberg, 1982) to Kaapvaal (Nixon et al., 1981; Boyd and Mertzmann, 1987). Vitim and Pali Aike (sources as in Fig. 3) show more enriched compositions; Jetty Peninsula SGL have similar CaO but lower Al_2O_3 contents to spinel–garnet lherzolites from Vitim and Pali Aike.

average Mg# range only between 90.7 and 91.4 in seven samples, whereas CaO contents are generally <0.1% but occassionally much lower (<0.01%). There are small but systematic differences in the compositions of olivines between the groups: olivines from most CRSL exhibit lower Mg# (89.0–89.7), whereas two (U-36 and U-N1; Table 4) are in the same range (91.0–91.8) as the CPSL. The group average is lower (Mg# = 90.3) than for CPSL (Mg# = 91.0). Olivines from spinel–garnet lherzolites generally have Mg# within the range 90–91, intermediate between the populations of the other two groups; the group average of 90.0 is marginally lower than for the CRSL. Small olivine neoblasts adjacent to orthopyroxene in SGL sample U-16 have lower Mg# (89.2–90.0; Table 5).

5.2. Orthopyroxene

Orthopyroxene Mg# presents the same picture as that for olivines: the range is small relative to peridotite xenoliths around the world but varies systematically with decreasing Mg# from CPSL (average 91.7) through CRSL (90.6) to SGL (90.4). Orthopyroxenes from the CPSL possess the lowest Al_2O_3 (average 3.5%) amongst the three peridotite groups, and this oxide generally increases in abundance, through the CRSL to the SGL. As for olivine, orthopyroxenes show the greatest compositional range in the CRSL. The CPSL orthopyroxenes are typical of mantle spinel peridotites worldwide, although Cr_2O_3 contents are slightly higher and TiO_2 contents considerably lower. A good correlation between Mg# in opx with that in olivine indicates a close approach to equilibrium of major elements between the texturally primary phases in all rock groups in most cases, and a general coherence within all three groups. Small second-generation orthopyroxene crystals occur in spinel–garnet lherzolites as breakdown products of garnet in kelyphite rims. These orthopyroxenes are characterized by very high Al_2O_3 contents (10.5–14.7%), high CaO (1.34–2.57 wt%), and lower Mg# (81.8–88.5) relative to primary orthopyroxenes (Tables 4 and 5), as governed by the composition of the destabilized garnet.

5.3. Clinopyroxene

Clinopyroxene-poor spinel lherzolites contain only one generation of clinopyroxene characterized by low Na_2O (average 0.72%) and Al_2O_3 (3.0–4.4%). Together with the high Mg# (average 92.7; Table 4), this attests to their relatively depleted nature. The clinopyroxene-rich spinel lherzolites contain two generations of clinopyroxene as main populations throughout the rocks (Fig. 2b). The texturally primary clinopyroxenes are chrome-diopsides with much higher contents of TiO_2 (up to 0.64%, average 0.46%), Al_2O_3 (average 5.9%) and Na_2O (average 1.4%). Mg# of clinopyroxenes shows the same relationships between the groups as for olivine and orthopyroxene: CPSL are distinguished primarily by their higher Mg#, whereas CRSL and SGL show considerable overlap. In a plot of Al_2O_3 against Cr_2O_3, clinopyroxenes from CPSL show similar Al_2O_3 and slightly lower Cr_2O_3 relative to xenoliths from Pali Aike, whereas spinel + garnet lherzolites are considerably more Al_2O_3-rich, although similar to the SGL from Vitim (Fig. 5). There is generally a similar distinction between garnet-bearing and garnet-free spinel lherzolites as for Pali Aike. The distinction from cratonic peridotites by high Al_2O_3 is as clear for the Jetty Peninsula SGL as for the other SGL from non-cratonic sources (Fig. 5).

The recrystallized rims of clinopyroxenes are chemically different, with lower Na_2O (0.29–0.88%; average 0.57%) and Al_2O_3 (average 4.7%) than primary clinopyroxenes. Mg# values are generally higher (average 91.5) than for primary clinopyroxenes (90.4). In the SGL, clinopyroxene rims are developed only sporadically; where present, they have the same chemical characteristics as clinopyroxene rims in the CRSL, but contain higher amounts of MnO derived from higher concentrations in the parental clinopyroxenes. Rare clinopyroxene neoblasts around orthopyroxene in SGL are generally lower in non-quadrilateral cations than other clinopyroxene generations, with the

Table 4
Electron microprobe analyses of minerals in Jetty Peninsula peridotites

Group	Sample #	Mineral	SiO_2	TiO_2	Al_2O_3	Cr_2O_3	FeO	MnO	MgO	NiO	CaO	Na_2O	K_2O	Total	Mg#	Cr#
SGL	U-16	Olivine	40.69	0.035	0.043	0.053	9.47	0.158	47.76	0.31	0.14	0.015		98.68	90.0	
SGL	U-17	Olivine	40.28	0.010	0.046	0.066	9.36	0.131	48.46	0.41	0.11	0.021		98.89	90.2	
SGL	U-47	Olivine	41.11	0.005	0.045	0.032	9.92	0.138	48.53	0.34	0.07	0.010		100.19	89.7	
SGL	U-3/3A	Olivine	41.19	0.006	0.076	0.057	9.78	0.127	48.81	0.37	0.12	0.015		100.54	89.9	
SGL	D-3	Olivine	41.17	0.008	0.057	0.052	9.04	0.163	50.43	0.42	0.13	0.017		101.49	90.9	
SGL	DK-8/3	Olivine	41.56	0.018	0.043	0.019	9.63	0.387	49.63	0.13	0.09	0.013		101.53	90.2	
SGL	D-N1	Olivine	40.13	0.006	0.068	0.061	9.76	0.156	48.19	0.37	0.12	0.019		98.87	89.8	
SGL	D-N4	Olivine	40.76	0.014	0.064	0.022	10.15	0.141	49.05	0.37	0.10	0.017		100.69	89.6	
SGL	XLT-1	Olivine	41.80	0.009	0.038	0.051	9.89	0.132	49.75	0.37	0.11	0.012		102.16	90.0	
SGL	3/1-3	Olivine	40.65	0.030	0.088	0.023	9.51	0.170	48.92	0.39	0.12	0.023		99.91	90.2	
SGL	15/1-2	Olivine	40.74	0.018	0.167	0.064	9.61	0.166	49.35	0.34	0.14	0.014		100.61	90.2	
CRSL	U-1	Olivine	39.97	0.012	0.034	0.055	8.90	0.171	50.15	0.36	0.10	0.014		99.76	90.9	
CRSL	U-36	Olivine	40.83	0.020	0.035	0.030	8.06	0.185	50.11	0.37	0.10	0.030		99.76	91.7	
CRSL	U-N1	Olivine	40.15	0.018	0.034	0.024	8.56	0.132	48.40	0.36	0.10	0.014		97.80	91.0	
CRSL	U-4/9-2	Olivine	41.32	0.022	0.024	0.053	10.51	0.120	48.57	0.38	0.09	0.001		101.09	89.2	
CRSL	XLT-4	Olivine	41.46	0.017	0.046	0.048	10.31	0.144	49.16	0.37	0.03	0.016		101.67	89.5	
CRSL	XLT-5	Olivine	41.45	0.024	0.009		10.04	0.127	49.12	0.38	0.03	0.013		101.16	89.7	
CPSL	U-3	Olivine	41.00	0.008	0.042	0.049	8.59	0.134	50.10	0.37	0.096	0.010		100.40	91.2	
CPSL	U-3/4-2	Olivine	41.55	0.024	0.025	0.022	8.88	0.118	49.77	0.39	0.077	0.011		100.86	90.9	
CPSL	D-11	Olivine	40.06	0.017	0.018	0.158	8.85	0.210	48.65	0.37	0.072	0.010		98.41	90.7	
CPSL	D-24	Olivine	40.53	0.012	0.031	0.031	8.38	0.180	48.84	0.37	0.079	0.005		98.46	91.2	
CPSL	D-N2	Olivine	40.26	0.035	0.038	0.072	8.70	0.168	49.13	0.40	0.086	0.015		98.90	91.0	
CPSL	1/4-3	Olivine	40.96	0.030	0.021	0.080	8.82	0.180	50.32	0.39	0.058	0.014		100.86	91.0	
CPSL	32601-9B	Olivine	41.62	0.016	0.016	0.016	8.60	0.416	50.19	0.33	0.018	0.008		101.00	91.2	
SGL	U-16	Opx	54.33	0.076	5.05	0.707	5.94	0.171	32.21	0.106	1.18	0.143		99.92	90.6	
SGL	U-17	Opx	53.61	0.258	4.68	0.651	5.89	0.166	31.92	0.099	1.05	0.144		98.47	90.6	
SGL	U-47	Opx	55.39	0.065	4.36	0.606	6.26	0.127	32.49	0.093	0.85	0.121	0.005	100.37	90.2	
SGL	U-3/3A	Opx	54.51	0.138	5.96	0.665	6.07	0.129	31.65	0.106	1.39	0.184	0.008	100.81	90.3	
SGL	D-3	Opx	54.23	0.134	5.64	0.689	5.66	0.159	32.47	0.101	1.18	0.161		100.43	91.1	
SGL	DK-8/3	Opx	55.50	0.102	4.88	0.700	6.04	0.111	32.71	0.124	1.10	0.125	0.005	101.39	90.6	
SGL	D-N1	Opx	53.40	0.159	5.54	0.657	6.16	0.153	31.34	0.115	1.20	0.177		98.90	90.1	
SGL	D-N4	Opx	54.72	0.203	5.02	0.690	6.29	0.166	32.24	0.117	1.15	0.178		100.77	90.1	
SGL	XLT-1	Opx	55.61	0.071	5.06	0.713	6.29	0.122	32.58	0.104	1.16	0.175	0.005	101.89	90.2	
SGL	3/1-3	Opx	53.92	0.166	5.75	0.689	6.07	0.149	31.80	0.108	1.26	0.160		100.08	90.3	
SGL	15/1-2	Opx	53.86	0.167	5.98	0.697	5.94	0.154	31.74	0.116	1.41	0.185		100.25	90.5	
CRSL	U-1	Opx	54.37	0.035	4.26	0.663	5.65	0.154	33.41	0.096	1.01	0.102		99.75	91.3	
CRSL	U-36	Opx	54.87	0.207	4.74	0.713	5.19	0.157	33.07	0.112	1.14	0.180		100.39	91.9	
CRSL	U-N1	Opx	53.83	0.133	4.96	0.680	5.45	0.130	31.80	0.115	1.07	0.158		98.33	91.2	
CRSL	U-4/9-2	Opx	54.86	0.191	4.62	0.715	6.59	0.099	31.92	0.150	1.09	0.151	0.003	100.38	89.6	
CRSL	XLT-4	Opx	55.45	0.170	4.50	0.769	6.54	0.136	32.44	0.113	1.14	0.120	0.006	101.38	89.8	
CRSL	XLT-5	Opx	56.24	0.084	3.86	0.252	6.97	0.149	33.47	0.066	0.34	0.035	0.008	101.47	89.5	
CPSL	U-3	Opx	55.46	0.023	3.83	0.748	5.40	0.154	33.59	0.104	0.96	0.071		100.34	91.7	
CPSL	U-3/4-2	Opx	56.05	0.012	3.88	0.622	5.63	0.130	33.53	0.103	0.88	0.079	0.005	100.92	91.4	
CPSL	D-11	Opx	54.67	0.026	3.63	0.535	5.34	0.128	32.87	0.105	0.84	0.040		98.17	91.7	
CPSL	D-24	Opx	55.45	0.017	3.54	0.592	5.16	0.134	32.91	0.101	0.90	0.040		98.84	91.9	
CPSL	D-N2	Opx	54.72	0.020	3.51	0.672	5.38	0.194	33.14	0.136	0.94	0.076		98.79	91.7	
CPSL	1/4-3	Opx	55.76	0.028	3.70	0.573	5.41	0.168	33.85	0.120	0.88	0.060		100.54	91.8	
CPSL	32601-9B	Opx	57.33	0.022	2.44	0.401	5.72	0.081	34.71	0.142	0.38	0.016	0.010	101.25	91.5	
SGL	U-16	Cpx	51.66	0.387	4.52	1.18	3.29	0.108	16.88	0.047	20.80	0.78		99.66	90.1	
SGL	U-17	Cpx	50.53	0.716	6.44	1.21	3.13	0.116	15.72	0.070	19.02	1.47		98.42	89.9	
SGL	U-47	Cpx	52.58	0.180	5.67	1.22	3.05	0.086	15.85	0.029	20.11	1.59	0.010	100.38	90.3	
SGL	U-3/3A	Cpx	51.55	0.325	7.40	1.04	3.55	0.116	17.02	0.087	18.12	1.26	0.005	100.49	89.5	
SGL	D-3	Cpx	51.58	0.415	6.94	1.19	3.25	0.110	16.60	0.042	18.43	1.43		99.98	90.1	
SGL	DK-8/3	Cpx	52.82	0.266	5.44	1.32	3.03	0.073	16.68	0.097	20.63	1.29	0.003	101.64	90.8	
SGL	D-N1	Cpx	50.72	0.478	6.94	1.35	3.60	0.094	15.98	0.046	18.33	1.55		99.07	88.8	
SGL	D-N4	Cpx	51.40	0.608	6.85	1.19	3.73	0.177	16.63	0.056	18.54	1.22		100.41	88.8	
SGL	XLT-1	Cpx	53.12	0.197	6.22	1.47	3.46	0.106	16.88	0.080	19.23	1.53	0.009	102.31	89.7	
SGL	3/1-3	Cpx	51.32	0.502	7.00	1.14	3.39	0.121	16.25	0.061	18.18	1.44		99.39	89.5	
SGL	15/1-2	Cpx	51.47	0.442	7.26	1.13	3.55	0.118	17.05	0.070	17.56	1.30		99.95	89.5	
CRSL	U-1	Cpx	51.56	0.063	5.02	1.11	2.84	0.125	16.89	0.051	20.05	1.14		98.85	91.4	
CRSL	U-36	Cpx	51.74	0.638	6.38	1.30	2.96	0.075	16.33	0.053	19.02	1.62		100.11	90.8	
CRSL	U-N1	Cpx	51.19	0.388	5.69	1.22	2.82	0.074	16.21	0.071	19.93	1.22		98.80	91.1	
CRSL	U-4/9-2	Cpx	52.13	0.595	5.93	1.29	3.68	0.093	16.29	0.015	19.22	1.46		100.70	88.7	

(*continued on next page*)

Table 4 (*continued*)

Group	Sample #	Mineral	SiO_2	TiO_2	Al_2O_3	Cr_2O_3	FeO	MnO	MgO	NiO	CaO	Na_2O	K_2O	Total	Mg#	Cr#
CRSL	XLT-4	Cpx	52.62	0.435	5.37	1.14	3.54	0.095	16.73	0.041	20.30	1.16	0.009	101.44	89.4	
CRSL	XLT-5	Cpx	52.77	0.634	6.83	0.72	2.21	0.063	14.22	0.016	22.14	1.96	0.010	101.57	92.0	
CPSL	U-3	Cpx	52.95	0.061	4.24	1.15	2.77	0.102	17.40	0.073	20.46	0.80		100.01	91.8	
CPSL	U-3/4-2	Cpx	53.69	0.040	4.25	0.99	2.65	0.078	17.26	0.062	21.62	0.84	0.008	101.48	92.1	
CPSL	D-11	Cpx	51.73	0.047	3.75	0.81	2.28	0.084	16.86	0.038	22.05	0.63		98.28	93.0	
CPSL	D-24	Cpx	52.27	0.000	3.65	0.97	2.29	0.069	17.05	0.065	21.88	0.58		98.83	93.0	
CPSL	D-N2	Cpx	52.25	0.040	3.80	1.14	2.50	0.090	17.24	0.063	21.58	0.76		99.46	92.5	
CPSL	1/4-3	Cpx	53.30	0.040	3.85	0.99	2.40	0.066	17.33	0.052	21.35	0.81		100.20	92.8	
CPSL	32601-9B	Cpx	53.90	0.037	2.95	0.91	1.84	0.038	16.59	0.061	24.97	0.61	0.005	101.91	94.1	
SGL	U-16	Garnet	42.04	0.130	22.32	1.91	6.83	0.367	20.54		5.57	0.013		99.72	84.3	
SGL	U-17	Garnet	41.78	0.135	21.61	1.50	7.55	0.405	21.28		5.54			99.79	83.4	
SGL	U-47	Garnet	41.74	0.250	21.25	1.89	8.19	0.340	21.08		5.24	0.030		99.99	82.1	
SGL	U-3/3A	Garnet	45.06	0.155	19.32	1.68	6.77	0.268	24.74	0.058	3.44	0.049		101.54	86.7	
SGL	D-3	Garnet	41.57	0.320	22.93	1.11	6.29	0.540	21.89		5.04			99.69	86.1	
SGL	DK-8/3	Garnet	43.40	0.173	21.39	1.99	8.25		23.08		4.18	0.013		102.47	83.3	
SGL	D-N1	Garnet	41.78	0.135	21.61	1.50	7.73	0.405	21.28		5.54	0.015		99.98	83.1	
SGL	D-N4	Garnet	41.78	0.135	21.61	1.50	7.73	0.405	21.28		5.54	0.015		99.98	83.1	
SGL	XLT-1	Garnet	42.88	0.054	17.67	1.43	7.41	0.278	27.25	0.047	1.34	0.014		98.36	86.8	
SGL	3/1-3	Garnet	41.59	0.205	22.30	1.85	7.06	0.285	21.44		5.30			100.02	84.4	
SGL	15/1-2	Garnet	41.54	0.240	22.38	1.44	6.35	0.315	20.52	0.040	5.42	0.015		98.25	85.2	
SGL	U-16	Spinel		0.14	49.2	17.1	11.50	0.18	19.3	0.305				97.71	74.9	18.8
SGL	U-17	Spinel		0.53	49.3	16.1	11.85	0.18	18.9	0.323				97.16	74.0	17.9
SGL	U-47	Spinel	0.07	0.14	46.4	20.8	12.89	0.20	18.7	0.238				99.41	72.1	23.1
SGL	U-3/3A	Spinel	0.17	0.21	54.3	12.8	11.19	0.18	20.7	0.360				99.98	76.7	13.6
SGL	D-3	Spinel		0.26	50.3	16.0	11.22	0.15	20.5	0.342				98.69	76.5	17.5
SGL	DK-8/3	Spinel	0.11	0.22	48.7	19.9	12.32	0.27	19.4	0.197				101.12	73.7	21.4
SGL	D-N1	Spinel		0.39	47.6	16.8	12.29	0.16	18.9	0.330				96.51	73.3	19.1
SGL	D-N4	Spinel		0.44	50.4	15.3	12.31	0.21	19.0	0.356				98.00	73.3	16.8
SGL	XLT-1	Spinel	0.14	0.14	51.8	16.1	12.29	0.15	20.3	0.340				101.28	74.6	17.2
SGL	3/1-3	Spinel		0.33	50.7	15.0	11.55	0.10	19.8	0.343				97.84	75.4	16.5
SGL	15/1-2	Spinel		0.27	53.2	13.3	10.73	0.10	20.7	0.367				98.69	77.5	14.3
CRSL	U-1	Spinel		0.05	43.2	23.3	12.61	0.18	18.7	0.262				98.30	72.6	26.4
CRSL	U-36	Spinel		0.60	44.0	21.4	11.25	0.07	19.8	0.315				97.43	75.8	24.5
CRSL	U-N1	Spinel		0.25	47.6	18.4	10.87	0.09	19.2	0.352				96.77	75.9	20.5
CRSL	U-4/9-2	Spinel	0.09	0.63	42.4	23.2	14.73	0.22	18.2	0.376				99.85	68.8	26.7
CRSL	XLT-4	Spinel	0.11	0.57	40.8	25.4	15.50	0.24	17.8	0.264				100.62	67.1	29.4
CRSL	XLT-5	Spinel	0.02	0.04	59.6	9.1	11.67	0.13	19.8	0.361				100.71	75.2	9.2
CPSL	U-3	Spinel		0.08	39.2	27.9	12.59	0.14	18.2	0.269				98.35	72.0	32.2
CPSL	U-3/4-2	Spinel	0.08	0.04	42.9	25.4	12.49	0.22	18.7	0.276				100.09	72.8	28.3
CPSL	D-11	Spinel		0.02	44.3	23.3	10.64	0.10	18.2	0.255				96.81	75.3	25.9
CPSL	D-24	Spinel		0.02	41.6	25.1	10.45	0.11	18.0	0.264				95.52	75.5	28.7
CPSL	D-N2	Spinel		0.06	37.6	29.8	12.29	0.18	17.4	0.297				97.60	71.6	34.6
CPSL	1/4-3	Spinel		0.04	40.9	26.0	12.73	0.12	18.3	0.254				98.34	71.9	29.7
CPSL	32601-9B	Spinel	0.02	0.03	39.5	29.2	15.44	0.23	15.6	0.180				100.21	64.4	33.0

exception of TiO_2, which is higher (average 0.79 vs. 0.45 wt%). Clinopyroxenes in kelyphite rims around garnet contain low SiO_2 (mostly 47.1–48.0%) and Na_2O, but very high Al_2O_3 (mostly 10.4–11.6%). The Cr_2O_3-content is relatively low (0.34–0.68%), and Mg# ranges from 86.2 to 86.6, reflecting the lower Mg# of the parental garnet.

All these generations of clinopyroxene are easily distinguished from those originating from the host alkali picrite magma, which are present in rare patches and veinlets of infiltrating host material. Here, clinopyroxenes are brownish prismatic crystals rich in TiO_2 (4.5–5.8%), Al_2O_3 (7.6–9.5%) with Mg# ranging between 73.8 and 79.3. These markedly different compositional features are similar to those of host magma clinopyroxenes, confirming that infiltration of host magma material in other samples could be easily recognized.

5.4. Garnet

The occurrence of garnet is limited to relict grains inside kelyphite aggregates. Only a few analyses could be obtained (Table 4), because the replacement of garnet by kelphite is often complete. The garnets are pyrope-rich and similar in composition to those from other localities where spinel+garnet lherzolites are found in off-craton areas (Ionov et al., 1993; Xu et al., 1998; Glaser et al., 1999; Kempton et al., 1999a). In contrast, cratonic garnet lherzolites have higher Cr_2O_3, generally above 4% (Boyd and Mertzmann, 1987; Boyd et al., 1997; McDonough and Rudnick, 1998). Garnets from two samples deviate from the norm in having subcalcic compositions more typical of harzburgites, but they are not Cr_2O_3-rich as in G10 garnets (Jacob et al., 1997; Stachel et al., 1998). Their bulk

Table 5
Microprobe analyses of late-stage minerals in the Jetty Peninsula peridotites

Group	Sample #	Mineral	Textural position	SiO_2	TiO_2	Al_2O_3	Cr_2O_3	FeO	MnO	MgO	NiO	CaO	Na_2O	K_2O	Total	Mg#
SGL	U-16	Olivine	Neoblast	42.96		0.05	0.009	9.28	0.17	46.80	0.41	0.11			99.79	90.0
SGL	U-16	Olivine	Neoblast	40.44		0.02	0.13	10.41	0.2	48.31	0.13	0.23			99.87	89.2
SGL	U-16	Cpx	Neoblast	49.92	1.30	4.57	0.44	4.31	0.11	16.59	0.06	22.09	0.22		99.61	87.3
SGL	U-16	Cpx	Neoblast	53.00	0.46	2.22	0.96	3.72	0.19	19.04	0.01	20.19	0.26		100.05	90.1
SGL	U-16	Cpx	Neoblast	51.18	1.16	3.89	0.44	3.92	0.04	16.06	0.05	22.76	0.25		99.75	88.0
SGL	U-16	Cpx	Neoblast	51.57	0.22	3.81	1.62	2.96	0.08	16.91	0.01	22.28	0.29		99.75	91.1
CRSL	U-1	Cpx	Rim	52.13	0.05	2.87	1.36	2.85	0.11	18.70	0.032	21.55	0.31		99.96	92.1
CRSL	U-4/9-2	Cpx	Rim	51.30	0.53	4.49	1.53	3.30	0.11	16.82	0.079	21.30	0.55		100.01	90.1
CRSL	U-36	Cpx	Rim	51.88	0.53	3.89	1.60	2.54	0.07	17.30	0.080	21.90	0.48		100.27	92.4
CRSL	U-N1	Cpx	Rim	51.40	0.31	4.81	1.33	2.79	0.22	16.80	0.030	21.33	0.76		99.78	91.5
CRSL	XLT-4	Cpx	Rim	51.65	0.45	4.13	1.50	3.26	0.11	17.13	0.087	21.15	0.44		99.91	90.4
CRSL	XLT-5	Cpx	Rim	51.09	0.62	5.83	0.90	2.41	0.08	15.78	0.051	22.28	0.87		99.91	92.1
CRSL	XLT-5	Cpx	Rim	51.91	0.64	6.63	0.69	2.20	0.06	14.02		21.96	1.97		100.08	91.9
CRSL	U-1	Spinel	Rim		0.06	39.64	28.23	12.86	0.16	18.78	0.23				99.95	72.2
CRSL	U-1	Spinel	Rim		0.17	38.56	28.94	13.55	0.13	18.37	0.22				99.94	70.7
CRSL	U-36	Spinel	Rim		1.05	37.38	28.93	12.98	0.14	19.29	0.30				100.07	72.6
CRSL	U-36	Spinel	Rim		0.95	40.84	25.69	11.92	0.16	19.88	0.36				99.80	74.8
SGL	U-16	Cpx	Rim	51.36	0.23	3.79	1.42	3.18	0.15	17.14	0.09	21.94	0.37		99.67	90.6
SGL	U-17	Cpx	Rim	51.87	0.65	4.81	1.38	3.13	0.15	18.08	0.04	19.26	0.57		99.94	91.1
SGL	D-3	Cpx	Rim	51.82	0.30	4.78	1.30	3.09	0.10	18.04	0.04	19.71	0.51		99.69	91.2
SGL	D-N1	Cpx	Rim	51.56	0.52	3.94	1.31	3.58	0.15	17.32	0.01	21.01	0.61		100.01	89.6
SGL	D-N4	Cpx	Rim	51.68	0.54	3.95	1.49	3.38	0.07	17.67	0.08	20.59	0.45		99.90	90.3
SGL	3/1-3	Cpx	Rim	50.96	0.54	5.27	1.60	3.29	0.10	16.93		20.88	0.43		100.00	90.2
SGL	15/1-2	Cpx	Rim	51.52	0.40	5.28	1.17	3.31	0.17	17.54	0.01	20.04	0.46		99.91	90.4
SGL	DK-8/3	Spinel	Rim		0.218	46.71	20.60	12.8	0.31	19.23	0.18				100.05	72.8
SGL	D-N1	Spinel	Rim		0.74	43.58	21.88	14.79	0.06	18.36	0.30				99.71	68.9
SGL	XLT-1	Spinel	Rim		0.153	49.29	17.55	13.1	0.16	19.5	0.34				100.09	72.6
SGL	D-N4	Opx	Kelyphite	51.64	0.19	9.02	0.51	7.13	0.48	29.27	0.09	1.55	0.02		99.91	88.0
SGL	D-N4	Opx	Kelyphite	49.94	0.28	11.26	0.92	6.66	0.46	28.86	0.05	1.58	0.04		100.05	88.5
SGL	U-17	Opx	Kelyphite	47.62	0.13	14.49	1.25	7.01	0.46	26.97	0.05	1.63	0.05		99.66	87.3
SGL	U-47	Opx	Kelyphite	50.09	0.09	10.05	0.71	10.19	0.50	25.67	0.04	2.34	0.01		99.68	81.8
SGL	DK-8/3	Opx	Kelyphite	48.63	0.11	13.68	1.19	7.33		26.86	0.36	1.94	0.01		100.10	86.7
SGL	D-N1	Opx	Kelyphite	48.20	0.12	13.75	1.18	7.23	0.46	26.35		2.30	0.15		99.74	86.7
SGL	D-N4	Cpx	Kelyphite	47.50	0.46	11.58	0.68	4.17	0.20	15.15	0.02	20.13	0.15		100.05	86.6
SGL	U-17	Cpx	Kelyphite	48.03	0.47	10.62	0.35	4.43	0.50	15.52	0.01	19.90	0.03		99.86	86.2
SGL	U-17	Cpx	Kelyphite	47.07	0.46	10.41	0.34	4.34	0.491	15.21	0.010	19.50	0.03		97.87	86.2
SGL	D-N1	Cpx	Kelyphite	51.03	0.57	5.33	1.33	3.74	0.117	16.92	0.085	19.59	0.83		99.54	89.0
SGL	D-N4	Spinel	Kelyphite		0.07	62.62	5.52	9.60	0.26	21.48	0.16				99.71	79.9
SGL	U-17	Spinel	Kelyphite		0.04	60.71	7.96	10.06	0.44	20.48	0.06				99.75	78.4
SGL	U-17	Spinel	Kelyphite		0.03	60.5	7.03	10.43	0.27	20.31	0.05				98.62	77.6
SGL	U-47	Spinel	Kelyphite		0.06	62.79	5.07	11.37	0.23	19.97	0.15				99.63	75.8
SGL	DK-8/3	Spinel	Kelyphite		0.03	61.09	7.94	9.85	0.04	20.61	0.29				99.85	78.9
SGL	D-N1	Spinel	Kelyphite		0.04	60.03	7.08	10.78	0.32	20.69	0.03				98.97	77.4
SGL	D-N1	Spinel	Kelyphite			59.3	7.39	10.50	0.33	19.97	0.03				97.51	77.2
SGL	XLT1	Spinel	Kelyphite			58.7	7.70	9.68	0.43	19.80	0.06				96.37	78.5

rock compositions are also not unusual. Garnets from sample U-3/3A show lower CaO (1.96%) and higher MgO (26.8%) towards the rims. This may be due to partial breakdown of the mineral during incipient kelyphite formation. Analyses of minerals formed during kelyphitic alteration are given in Table 5.

5.5. Spinel

Spinels in clinopyroxene-poor spinel lherzolites are generally Ti-poor ($\leqslant$0.09% TiO_2) and have Cr_2O_3 contents of 23–30% and Cr# [=100 Cr/(Cr + Al); cation ratios] of 25.9–33.0. The sequence CPSL through CRSL to SGL shows similar trends to those seen for olivine, clinopyroxene and orthopyroxene, namely decreasing degree of depletion of relatively fertile mantle. In particular, Cr# decreases from an average of 30.3 in the CPSL to 17.8 in the SGL with a concomitant slight increase in Mg# from 71.9 to 74.7. The dotted line drawn in Fig. 6 empirically separates spinels in garnet-free lherzolites from those in spinel–garnet lherzolites for those localities in which spinel–garnet lherzolites have been thoroughly investigated.

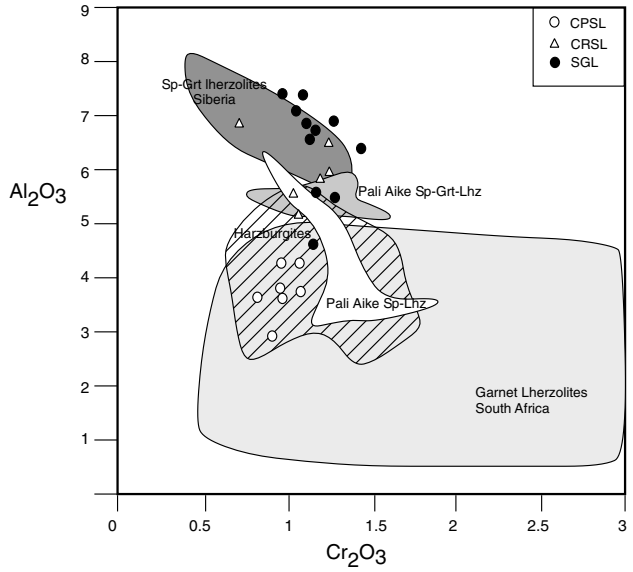

Fig. 5. Al_2O_3 and Cr_2O_3 contents of clinopyroxenes showing lower Al_2O_3 in spinel lherzolites relative to garnet-bearing lherzolites, reproducing the pattern seen at Pali Aike (Kempton et al., 1999a). Shaded field for harzburgites is also from South Africa (Kaapvaal). The Jetty Peninsula SGL clinopyroxenes have similarly high Al_2O_3 to SGL xenoliths from Vitim, Siberia, whereas the SL have slightly but consistently lower Cr_2O_3 than Pali Aike rocks. Sources and abbreviations as in Figs. 3 and 4.

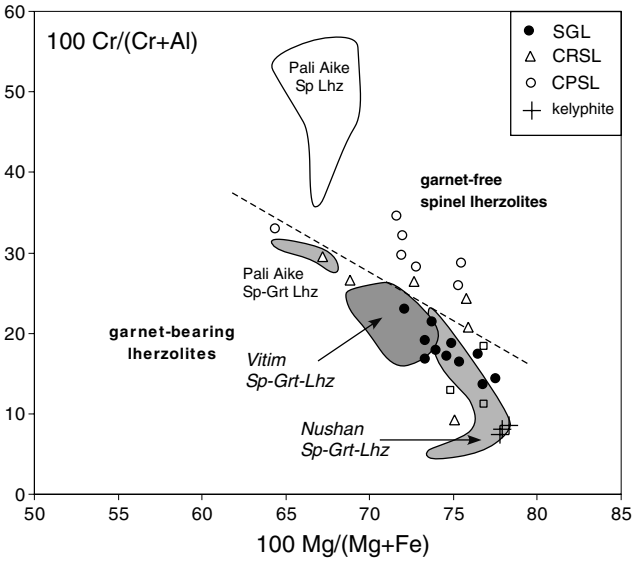

Fig. 6. Spinel compositions in Jetty Peninsula garnet-bearing xenoliths confirm the pattern seen in other spinel + garnet lherzolites, in that garnet-bearing can be distinguished from garnet-free spinel peridotites by lower Cr# and Mg# in spinels. The Jetty Peninsula spinels are offset to higher Mg# and lower Cr# relative to the Pali Aike rocks, but are more similar to rocks from Nushan and Vitim. Sources and abbreviations as in Figs. 3 and 4.

Recrystallized spinel rims from CRSL and SGL, where present, are characterized by erratically higher TiO_2 contents (0.06–1.05%) and slightly higher Cr# compared to primary spinels. Spinels in kelyphite rims have very low Cr_2O_3 (5.1–8.0%), high Al_2O_3 (58.7–62.4%) and consequently low Cr# of 5.1–8.0. In CPSL-sample 32601-9B, spinel compositions deviate from those in other CPSL samples: Mg# (64.4) and NiO (0.18 vs. >0.25%) are lower and MnO higher (0.23 vs <0.18%). The composition of spinel from CRSL-sample XLT-5 is unusual for garnet-free samples, with very low Cr# (9.1–9.3) which are comparable to spinel from kelyphites. However, no traces of garnet or kelyphite have been found in this sample.

5.6. Carbonates and sulphides

Sulphide minerals are preserved as blebs included in other minerals but have not been observed as independent interstitial phases. Their compositions are intermediate between pyrite and pentlandite and vary widely within a single inclusion. These blebs may represent droplets of immiscible sulphide liquids trapped by silicate mineral phases at mantle depth (Andersen et al., 1987). Carbonate minerals occur as inclusions in the rock-forming minerals or as rare interstitial patches in many samples of all three groups. Compositions are relatively uniform, corresponding to Fe- and Ca-bearing magnesites. Several inclusions of mainly Fe-magnesite composition (42.1–44.8% MgO, 3.0–7.1% FeO and 0.8–1.2% CaO) in orthopyroxene were found in CPSL, and a Fe-richer carbonate (28.6–34.6% MgO, 15.1–19.1% FeO and 3.6–6.7% CaO) was found coexisting with pentlandite inclusions in olivine.

5.7. Glass

Glass occurs in several textural and compositional forms within the Jetty Peninsula peridotite, namely in kelyphitic rims around garnet, in recrystallized clinopyroxene and spinel rims, as intergranular films between peridotite minerals, and rarely as interstitial pools. Representative analyses of these glass types are given in Table 6. In comparison to compositions of melts commonly considered to be in equilibrium with peridotite (Falloon et al., 1999), all these glasses are extremely enriched in Al_2O_3, and some have exceptionally low contents of MgO, FeO and K_2O.

The SiO_2 contents of glasses within kelyphite rims mantling garnet range from 51.0% to 53.5% and total alkali contents are <3% (Table 6). The glasses occur together with orthopyroxene, clinopyroxene and spinel listed in Table 5. Glass inside recrystallized rims of clinopyroxene has much higher total alkali contents (5.2–7.2%), whereby Na_2O dominates over K_2O (≤0.2%). Glassy films coating spinel (Fig. 2c) have SiO_2 contents of 60–61%, subequal Na_2O (4.1–4.3%) and K_2O (4.0–5.0%) contents, high Cr_2O_3 (1.6–1.9%) and appreciable P_2O_5 contents of 0.42–0.55%. Glass also occurs in films along grain boundaries between different silicate minerals in SGL, and contains 50–51% SiO_2, 2.7–4.1% Na_2O and very low contents of K_2O (0.04–0.07%). This glass is compositionally similar to that within clinopyroxene rims, especially in terms of Na_2O/K_2O, but displays somewhat higher amounts of FeO and

Table 6
Representative microprobe analyses of glasses in the Jetty Peninsula peridotites

Analysis	1	2	3	4	5	6	7	8	9	10	11	12
Glass type	Kelyphite	Kelyphite	Kelyphite	Cpx rim	Cpx rim	Cpx rim	Spinel rim	Spinel rim	Intergran. film	Intergran. film	Matrix	Matrix
Rock type	SGL	SGL	SGL	SGL	CRSL	CRSL	CPSL	CPSL	SGL	SGL	CRSL	CRSL
SiO_2	53.55	51.68	53.42	52.08	59.26	60.44	60.87	59.97	49.93	50.98	54.02	57.45
TiO_2	0.30	0.61	0.55	0.01	0.21	0.33	0.05	0.05	0.04	0.07	1.46	0.95
Al_2O_3	23.41	23.16	23.86	28.10	24.18	22.57	21.42	20.72	30.19	28.23	20.99	20.92
Cr_2O_3	0.03	0.32	0.09	0.04	0.02	0.04	1.91	1.64	0.38	0.14		0.03
FeO	3.10	4.73	3.86	0.40	1.78	0.78	0.89	1.07	0.75	0.60	2.53	2.48
MnO	0.26	0.31	0.09	0.08	0.04	0.01					0.11	0.09
NiO		0.07			0.03	0.01			0.03	0.14		0.03
MgO	3.34	5.68	3.52	0.78	1.21	2.09	1.85	2.17	0.71	1.27	3.64	2.35
CaO	13.38	13.00	11.64	12.54	7.23	5.47	2.11	2.57	15.03	12.15	5.15	4.08
Na_2O	0.26	0.25	1.07	5.24	6.78	6.95	4.29	4.15	2.60	4.05	2.68	3.52
K_2O	0.17	0.25	1.80	0.01	0.15	0.21	4.98	4.02	0.07	0.04	6.22	6.00
P_2O_5	0.10					0.01	0.55	0.42				
Total	97.90	100.06	99.90	99.28	100.89	98.91	98.92	96.78	99.73	97.67	96.80	97.90
Mg#	65.7	68.2	61.9	77.8	52.8	82.7	78.9	78.4	62.9	79.2	72.0	62.8

MgO, and lower Na_2O. There is no obvious reaction relationship between glass films and adjacent minerals, suggesting that they represent equilibrium conditions. Interstitial pools of light-brown glass containing small crystals of spinel, sanidine and carbonate occur in MSL sample U-36. This glass has SiO_2 contents of 54–57%, and total alkalis of 8.9–9.5% about two thirds of which is K_2O (6.0–6.2%). The glass patches contain abundant quenched material which falsifies the original composition of the melt. The glass has a rather evolved composition (up to 85% normative feldspars), corresponding approximately to phonolite, although Mg# is quite high (63–72).

6. Trace element composition of minerals

Analyses of trace elements in constituent minerals of the peridotite xenoliths by Laser-ICP-MS were undertaken in order to further investigate the chemical inhomogeneities apparent from the major elements. Emphasis was laid on the transition elements as these include compatible and mildly incompatible elements that could shed light on early depletion processes, and potentially differentiate between enrichment events. Also, many trace elements normally analysed in clinopyroxenes and amphiboles (e.g., REE, Rb, Ba; Zack et al., 1997; Bottazzi et al., 1999; Marks et al., 2004) were neglected as they were expected to be near or below detection limits in olivine and orthopyroxene, which were the main objects of study here. Trace elements were analysed with an Agilent 7500cs ICP-MS coupled to a New Wave 213 nm Laser at the University of Greifswald (Jacob, 2006) using NIST SRM 612 glasses as external standards and microprobe analyses on the same minerals as internal standards. Additional standard glasses (BCR-2) were analysed as unknowns to monitor possible instrumental drift. Representative results and values obtained for standard glasses with the same analytical set-up (Jacob, 2006) are given in Table 7. These are in all cases within 15% of the accepted values, and 59% of standard measurements are within 5%.

Results show that two groups of samples can be identified; low-Ca and high-Ca groups. These descriptions refer to the Ca contents in olivine and orthopyroxene, and not to the whole-rock CaO contents, which do *not* differ between sample groups (Table 3). The low-Ca group comprises clinopyroxene-poor spinel lherzolite 32601-9B and clinopyroxene-rich spinel lherzolites XLT-5 and XLT-4; none of the spinel–garnet lherzolites were found to belong to this group. The low-Ca group is characterized by olivines with distinctly lower concentrations of Ca than in the high-Ca group (average 280 vs. 891 ppm; ranges 160–348 and 770–1100 ppm). In addition, concentrations of Ti (11.1 vs. 43 ppm on average), V (0.83 vs. 5.7 ppm), Cr (17 vs. 219 ppm) and Zn (20 vs. 57 ppm) are consistently lower than in the high-Ca group (Fig. 7). Orthopyroxenes follow the same pattern (Ca 3330 vs. 8490 ppm) for Ti (460 vs. 820 ppm), Cr (1870 vs. 4010 ppm), and Zn (18 vs. 47 ppm), whereas Cu (0.61 vs. 1.9 ppm), Ni (480 vs. 710 ppm), Ga (2.0 vs. 3.6 ppm) and to a lesser extent Li (0.90 vs. 1.17 ppm) also have lower concentrations in the low-Ca group (Table 7; Fig. 8).

Trace element variations in olivine and orthopyroxene as a function of the presence or absence of clinopyroxene have not been studied systematically, and few data sets on these minerals in peridotites are available for comparison. The partitioning of transition elements between pyroxenes is known to be a function of temperature (Seitz et al., 1999), and many of the trace element variations seen here may be due to the lower temperatures in the low-Ca group: low Ca, Ti and Cr are also seen in olivines and orthoyproxenes of the Sulu ultra-high pressure tectonic block, whose equilibration temperatures overlap with those of the low-Ca group of the Jetty Peninsula xenoliths (780–960 °C; Zhang et al., 2005). However, the concentrations of some elements in the Jetty Peninsula peridotites (e.g., Ti in

Table 7
Representative trace element analyses of minerals in the Jetty Peninsula peridotite xenoliths concentrations given in ppm

Sample	Group	Mineral	Li	Ca	Sc	Ti	V	Cr	Mn	Co	Ni	Cu	Zn	Ga	Sr	Y	Zr	Nb	Ba
601-9B	CPSL	Olivine	1.02	129	5.7	4.8	0.32	12.5	774	120	2571	0.59	21.8	<0.066	0.1896	0.0734	8.11	<0.022	0.282
601-9B	CPSL	Olivine	1.02	111	5.1	4.2	0.30	4.9	824	119	2640	<0.051	20.2	0.052	0.028	0.011	0.021	<0.0128	<0.0229
U3/4-2	CPSL	Olivine	1.74	943	6.1	57	5.4	220	910	133	2525	1.5	58.3	0.11	0.106	0.16	16.6	<0.0126	0.07
U3/4-2	CPSL	Olivine	3.10	898	5.9	55	5.4	219	897	128	2446	1.3	52.5	0.08	1.31	0.26	54.1	0.09	0.49
XLT-4	CRSL	Olivine	1.36	225	2.9	24	1.35	59	951	124	2496	4.0	16.1	<0.065	0.42	0.31	43	<0.0124	0.20
XLT-4	CRSL	Olivine	1.57	49	2.8	8.6	1.38	19.2	975	124	2484	1.8	18.0	0.08	1.74	0.49	775	0.023	1.7
XLT-5	CRSL	Olivine	1.76	280	3.3	33.1	1.43	10.4	1056	126	2444	0.87	21.1	0.32	0.21	0.03	87	0.0064	0.068
XLT-5	CRSL	Olivine	1.93	179	3.0	4.46	0.21	4.5	1001	128	2597	1.37	27.3	<0.111	0.44	0.17	34	<0.028	0.099
UN-1	CRSL	Olivine	1.33	800	4.9	44	4.4	155	892	127	2569	1.3	47	<0.138	0.0521	0.32	0.4	<0.0204	<0.072
UN-1	CRSL	Olivine	1.28	922	4.9	45	4.6	154	922	129	2610	37	52	<0.141	0.157	0.75	61	0.043	0.129
U3/3a	SGL	Olivine	1.39	1201	5.3	38	7.3	235	1004	132	2463	3.2	52.0	0.17	0.39	0.086	3.1	<0.0086	0.153
U3/3a	SGL	Olivine	1.26	1149	5.8	35	6.8	227	1007	136	2508	1.9	53.3	0.17	0.39	0.101	5.1	<0.0179	0.146
DK 8/3	SGL	Olivine	1.44	723	4.8	38	5.0	168	969	130	2448	2.5	70.8	0.14	0.054	0.25	10.7	0.02	0.34
DK 8/3	SGL	Olivine	1.34	918	4.7	57	9.0	349	960	121	2341	1.9	46.8	0.29	0.048	0.048	0.35	<0.0106	0.22
XLT-1	SGL	Olivine	1.92	1107	5.18	28.2	5.8	261	1089	147	2841	1.42	58	0.23	0.45	0.74	0.49	<0.0196	0.332
XLT-1	SGL	Olivine	1.81	1057	5.89	31.8	6.0	261	1067	142	2742	1.45	85	0.13	0.061	0.18	195	<0.0137	0.040
601-9B	CPSL	Opx	0.93	2743	24	103	82	2399	970	42	459	0.13	17.1	1.32	0.125	0.140	1.03	<0.0061	<0.0119
U3/4-2	CPSL	Opx	1.48	8553	22.6	1144	98	4316	978	59	715	3.2	38	3.9	1.16	1.82	98	0.065	1.98
U3/4-2	CPSL	Opx	0.95	8864	23.2	1187	97	4343	988	60	713	2.4	47	3.8	1.00	1.92	158	0.066	0.94
XLT-4	CRSL	Opx	0.99	1227	16.2	550	76	1632	945	46	522	0.59	17.9	2.6	0.16	0.42	15.1	<0.0108	0.088
XLT-4	CRSL	Opx	0.71	4604	17.0	700	78	1570	992	47	495	0.65	23.4	2.7	0.40	1.06	39	0.065	0.998
XLT-5	CRSL	Opx	0.52	4104	18.6	799	79	1590	1019	45	508	0.22	18.7	2.3	0.22	1.24	3.1	0.019	<0.042
XLT-5	CRSL	Opx	1.05	2701	16.4	595	75	1439	1055	44	491	0.86	15.6	2.2	0.14	0.67	4.3	0.016	0.058
UN-1	CRSL	Opx	1.00	7526	19.2	969	90	3593	863	51	711	1.3	27	3.4	0.76	1.22	27.4	0.11	1.43
UN-1	CRSL	Opx	0.99	8318	18.1	919	91	3972	855	51	693	1.2	29	3.6	1.14	1.10	5.22	0.095	<0.028
U3/3a	SGL	Opx	1.79	9051	19.0	751	97	3543	849	55	739	2.3	39.3	4.4	1.38	1.21	17.5	0.04	0.23
U3/3a	SGL	Opx	1.81	9711	21.3	759	105	3759	887	53	706	1.5	27.6	4.3	0.70	1.48	7.1	0.04	0.14
DK 8/3	SGL	Opx	0.87	6688	16.3	693	93	3663	896	53	685	2.5	30	3.4	0.93	0.61	22	0.083	0.13
DK 8/3	SGL	Opx	1.01	7591	16.7	739	91	3380	908	52	671	1.9	48	3.2	0.52	0.63	12.8	0.083	0.34
XLT-1	SGL	Opx	1.09	9967	19.6	512	93	5319	939	56	741	0.75	33	3.3	1.27	0.87	6.34	0.079	0.63
XLT-1	SGL	Opx	1.06	9494	22.3	551	91	4941	943	54	740	1.24	38	3.14	0.53	0.99	10.2	0.072	4.23
U3/4-2	CPSL	Cpx	1.21		64	3454	222	8117	740	28.1	387	57	43	4.2	94	19.8	271	0.59	0.92
U3/4-2	CPSL	Cpx	1.27		62	3445	225	8114	793	27.3	410	2.1	13.7	4.4	96	19.3	72	0.56	0.26
XLT-4	CRSL	Cpx	0.30		77	3607	246	4661	529	14.7	227	22	16.3	3.2	62	26	56	0.036	5.7
XLT-5	CRSL	Cpx	0.48		84	4061	232	4268	526	14.1	207	2.0	4.7	2.7	68	27	75	0.043	0.160
XLT-5	CRSL	Cpx	0.51		86	4080	241	4489	532	14.4	204	1.4	7.1	2.9	67	27	40	0.037	0.036
UN-1	CRSL	Cpx	0.79		54	2895	201	6467	601	20	318	4.1	41	3.4	106	14.5	96	1.48	0.192
UN-1	CRSL	Cpx	0.95		54	2827	203	6527	599	20	320	1.7	9	3.4	104	14.1	241	1.45	0.274
DK 8/3	SGL	Cpx	0.99		45	2015	220	6635	651	26	344	3.2	29	3.6	49	7.5	48	1.06	0.21

DK 8/3	SGL	Cpx	0.91	45	2056	227	6844	621	21	338	1.9	8.3	3.3	50	6.8	19.6	1.00	0.12
XLT-1	SGL	Cpx	1.08	49	1331	202	9875	685	23	374	1.32	10.7	3.27	77	8.8	19.4	0.655	0.118
XLT-1	SGL	Cpx	0.90	48	1292	183	8545	634	21	327	1.2	9.0	3.0	77	8.7	21.0	0.662	0.133
NIST SRM 612	Recomm[a]		41.54	41.05	48.11	39.22	39.88	38.43	35.26	38.44	36.71	37.92	36.24	76.15	38.25	35.99	38.06	37.74
NIST SRM 612	This study		42.64	40.23	48.84	39.72	35.02	37.82	34.64	38.82	38.96	42.54	38.26	76.34	37.50	35.15	37.88	38.07
BCR-2	Rrecomm[a]		9.49	33.2	13667	421	16.9	1526	37.7	12.05	21.8	147		333	34.4	184	13.1	668
BCR-2	This study		10.8	32.97	13728	447	18.4	1620	38.92	13.4	22.0	169		324	30.4	161	12.4	663

Values for standards are averages on the same instrument (Jacob, 2006).
[a] Recommended values for NIST SRM 612 are from Pearce et al. (1997), whereas those for BCR-2 are as compiled by Jacob (2006).

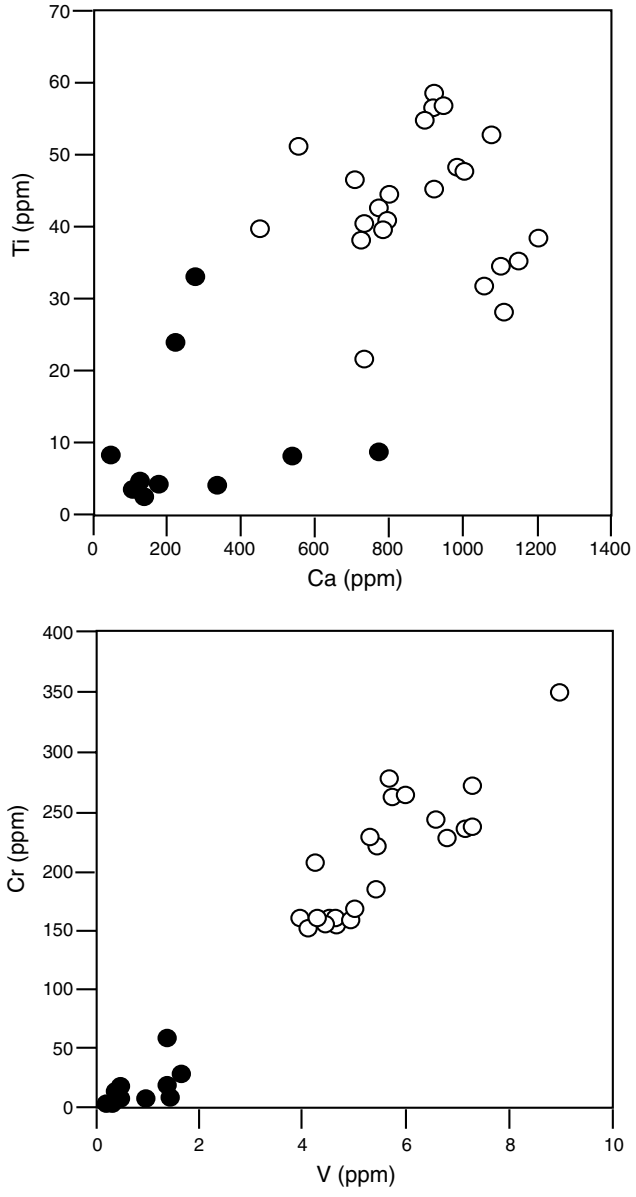

Fig. 7. Trace element compositions of olivines in Jetty Peninsula peridotite xenoliths. Solid circles are analyses of olivines in the low-Ca group (including both CPSL and CRSL, but no SGL), showing low concentrations of Ca, Ti, V and Cr. Open circles are from the high-Ca group. Data from Table 7.

olivine, Zn in both olivine and opx) are even lower than in the (clinopyroxene-bearing) Sulu rocks, which may be attributable to their depleted chemistry. Lithium concentrations are comparable to those generally seen in peridotitic olivines and orthoyproxenes (Seitz and Woodland, 2000; Seitz et al., 2004), with an average $D^{ol/opx}$ of 1.66.

Fewer analyses of clinopyroxenes were made; these are also presented in Table 7. These also show differences between the low-Ca and high-Ca sample groups noted above, but do not follow the same depletion and enrichment trends as for olivine and orthopyroxene: Sc (80 vs. 54 ppm), Ti (3830 vs. 2440 ppm) and Y (27 vs. 12.7 ppm) are enriched in cpx of the low-Ca sample group, whereas Li (0.38 vs. 1.05 ppm), Cr (4470 vs. 7570 ppm), Co (14.6

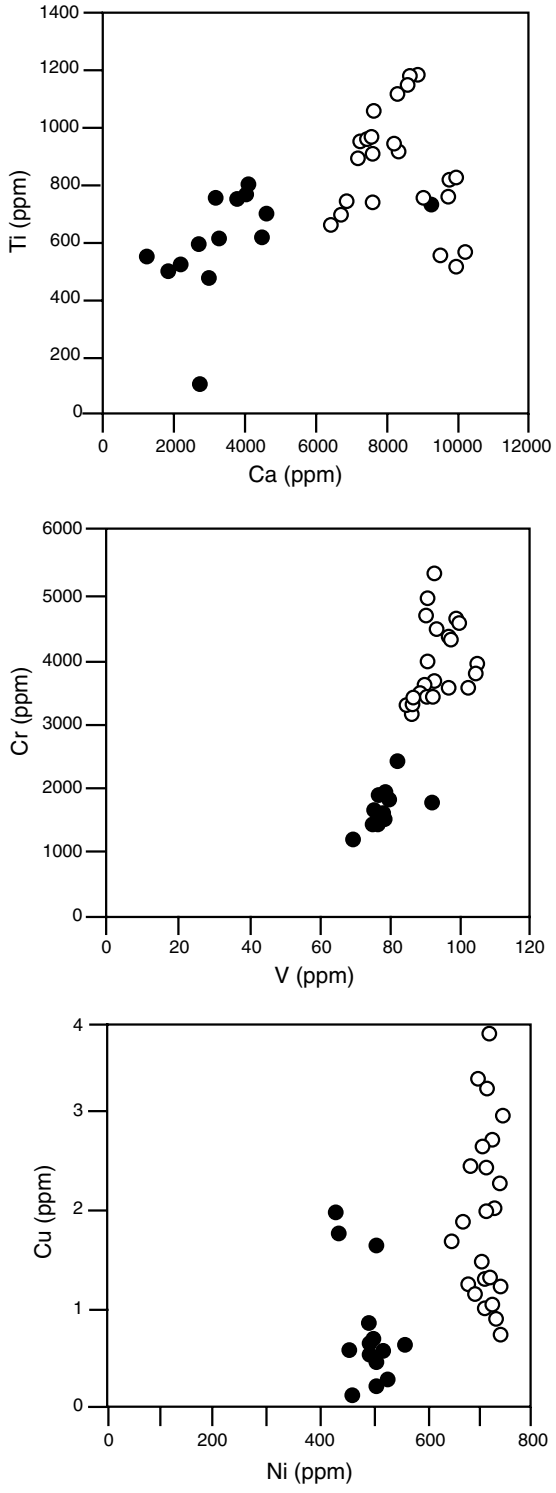

Fig. 8. Trace element compositions of orthopyroxenes in the Jetty Peninsula peridotite xenoliths. Solid circles, low-Ca group, open circles, high-Ca group. The first two panels show similar behaviour for Ca, Ti, Cr and V to olivines, whereas the difference in Cu and Ni is not seen in olivines. Data from Table 7.

vs. 23.3 ppm), Ni (220 vs. 350 ppm), Zn (11.1 vs. 18 ppm), Zr (54 vs. 159 ppm) and Nb (0.038 vs. 0.94 ppm) are depleted. Little difference is seen for V, Mn, Cu, Ga and Sr, whereas Ba varies erratically.

7. Discussion

The presence within one intrusive body of various xenolith types including both spinel- and garnet-bearing assemblages with varying degrees of re-enrichment testifies to a complex history of the upper mantle beneath the Jetty Peninsula. The petrographic and geochemical features of the rocks indicate an array of fairly primitive to depleted peridotite compositions, whereas other chemical and textural features are due to thermal perturbations which can be attributed to the rift margin setting. We first treat the interpretation of the mineral zonation and metasomatic effects and then discuss the mineralogical information about geothermal gradients in relation to possible past tectonic events.

7.1. Mineral zonation, recrystallization events and the origin of glasses

A combination of lines of evidence, including chemical zonation of major and trace elements in minerals, as well as recrystallized rims around clinopyroxenes and spinels (Fig. 2) enable several events in the mantle to be deciphered. It is important to avoid later confusion by noting that more than one of these relates to a "metasomatic" enrichment in the sense of Harte et al. (1993).

Recrystallized rims on minerals are commonly explained by the thermal influence of the host magma during ascent of xenoliths to the Earth's surface or by movement of the rocks to a higher level in the lithosphere (Frey and Green, 1974; Henjes-Kunst and Altherr, 1992). However, the presence within one intrusive body of groups both with (CRSL, SGL) and without (CPSL) such rims may be used to argue against recrystallization due to the thermal influence of the host magma. Furthermore, matrix glasses formed from infiltrating host melt have been identified (Table 6) and have compositions distinct from those associated with these rims. We argue that the rims were produced before incorporation of the xenoliths into the host magmas by a heating event in the mantle, probably related to the upward movement of the asthenosphere–lithosphere boundary during the early stages of development of the Lambert–Amery Rift. The higher concentrations of refractory elements and lower Na_2O and Al_2O_3 in the clinopyroxene rims in both CRSL and SGL compared to cores is consistent with loss of a melt component, and the glass inclusions within these rims are consistent with the interpretation that the clinopyroxenes melted. The low Na_2O contents (up to 1.5% in cores and as little as 0.3% Na_2O in rims) indicates little input of Na from elsewhere. Although the melting process may have been fluxed by a small volume external melt moving along grain boundaries, explaining the low but measurable K_2O content in the glass (<0.21 wt%) and the similarity in composition to intergranular melt films, the bulk of the melt inclusion material appears to come from the clinopyroxene.

Important information about the history of the mantle beneath the Jetty Peninsula can be gained from the garnets and their kelyphite rims. These show a two-stage history of garnet formation from spinel, followed by its subsequent breakdown leading to kelyphite formation around the garnets (Fig. 2f). A similar history has been described from Pali Aike and Chile (Kempton et al., 1999a) and Vitim, Siberia (Glaser et al., 1999), albeit from differing tectonic settings. The transformation of spinel peridotite to garnet peridotite can, in principle, be caused by either cooling or by a pressure increase. In both Pali Aike and Vitim, the formation of garnet from spinel is thought to be due to isobaric cooling rather than a pressure increase. Lee et al. (2001) described textures from Sierra Nevada mantle xenoliths, including garnet exsolution lamellae in clinopyroxene and garnets rimming spinels, which they interpreted to be caused by cooling into the garnet stability field. These features are not seen in the Jetty Peninsula peridotites, which may indicate a different mode of formation, namely an increase in pressure. This would be consistent with formation of garnet during a lithosphere thickening event such as collison, which is has been interpreted to have occurred in this region at about 1.1 Ga (Sheraton et al., 1993). The later garnet breakdown event could then have occurred at any stage of rift formation.

The dominance of subcalcic garnets in some samples (XLT-1 and U3/3A) shows that the garnets cannot be in equilibrium with clinopyroxene, and thus that the garnet formed in harzburgite, and clinopyroxene was introduced later, even though it now makes up >15% of the rock. The garnets are not Cr-rich and so did not form from Cr-rich spinel harzburgites at high pressures, as for G10 garnets (Bulatov et al., 1991; Jacob et al., 1997). Thus, the spinel harzburgites cannot have been much deeper than the pressure of 20–24 kbar given by geobarometric estimates, otherwise the parental spinels would have been much more Cr-rich (O'Neill, 1981; Klemme, 2002). Furthermore, this garnet formation occurred slowly enough to prevent the preservation of zoning in the minerals (Kempton et al., 1999a).

Explanations offered for the breakdown of garnet in the Pali Aike and Vitim rocks were both related to later heating associated with the upwelling of asthenospheric mantle. In Pali Aike this was attributed to back-arc extension (Kempton et al., 1999a), whereas in Vitim it was thought to be a distal effect of the development of sub-rift mantle, in effect the conversion of lithospheric mantle to asthenosphere (Glaser et al., 1999). In the Vitim xenoliths, it could also be demonstrated that kelyphite formation occurred *before* the metasomatic introduction of clinopyroxene and so definitely represents an event within the mantle. This is confirmed for kelyphites in the Jetty Peninsula peridotites, where rare examples of patches enriched in clinopyroxene and spinel close to thoroughly kelyphitized former garnets occur. These represent a grain coarsening stage involving the kelyphite-forming minerals after complete replacement of the garnet. This is worthy of note because kelyphite formation is often attributed to reaction with volatile-bearing infiltrating agents derived from the host magma (Dawson, 1980; Hunter and Taylor, 1982), and to be linked genetically with the emplacement of the magma (Garvie and Robinson, 1982).

The assemblage of orthopyroxene, clinopyroxene and spinel seen in the Jetty Peninsula kelyphites is a common breakdown reaction of garnet in kelyphites (e.g., Reid and Dawson, 1972; Glaser et al., 1999), whereas the occurrence of glass in kelyphites is rare. Hunter and Taylor (1982) describe glass in kelyphites from a kimberlite in Pennsylvania, ascribing their high alkali contents (6–9 wt%) to metasomatically introduced material. The lower, but nevertheless appreciable alkali contents in the Jetty Peninsula kelyphite glasses (up to >1% Na_2O; <2% K_2O) are difficult to explain in a completely closed system, but do not require much external material. The bulk of the glass composition can be explained by incongruent melting of garnet (Hunter and Taylor, 1982; Andronikov, 1997). A great variety of glass types have been described from mantle xenoliths around the world, and the involvement of hydrous phases in the production of these glasses is regularly invoked (Frey and Green, 1974; Yaxley et al., 1997). However, there is a strong indication that the mantle beneath the Jetty Peninsula represented by the current set of lherzolite xenoliths remained essentially dry: there are no convincing candidates for primary volatile-bearing phases unrelated to the host magma. The glasses occurring in interstitial pools and in reaction rims around spinels (Fig. 2c; Table 6) have the highest contents of both Na_2O and K_2O but are not associated with phlogopite or amphibole. They also have high SiO_2 and Al_2O_3 contents which may not be a primary feature of the melts but due to reaction with surrounding minerals (Zinngrebe and Foley, 1995; Schiano and Bourdon, 1999). In addition, the appreciable concentration of P_2O_5 (0.42–0.55%) in the glass rims around spinel indicates an external origin for this glass. These glassy films are interpreted to have originated by melt infiltration within the mantle: thin glass films have been described in experiments and from natural peridotites (Drury and FitzGerald, 1996; Franz and Wirth, 1997). The high alkali contents cannot be explained by any combination of primary mineral constituents of the peridotites, whereas enrichment of the glass in Cr_2O_3 reflects takeup of spinel components in the infiltating melt. An analogous reaction has been documented in the Inagli dunite of eastern Siberia, where Na-phlogopite has grown into adjacent olivine from the spinel-melt interface by incongruent dissolution (Zinngrebe, 1998). The infiltration of melt is expected to be promoted along spinel–silicate mineral interfaces due to the higher surface energy of the spinels (Schäfer and Foley, 2002), explaining its preferential occurrence here in the Jetty Peninsula xenoliths. The glasses in rims around clinopyroxene and as intergranular films have higher Na_2O/K_2O and are less likely to be affected by the host magma composition. They are believed to origi-

nate by incipient melting (see Franz and Wirth, 1997 for films), as indicated by the correspondingly lower Na_2O and Al_2O_3 in the clinopyroxene rims relative to the cores.

7.2. Oxidation state of the rifting mantle

The oxygen fugacity of the source of the Jetty Peninsula peridotite xenoliths was estimated using the olivine–orthopyroxene–spinel oxybarometer calibrated experimentally by Ballhaus et al. (1990). Fe^{3+} in spinel calculated assuming stoichiometry was used in the calculation as this is known to agree well with results from Mössbauer spectroscopy for all but very low Fe^{3+}/Fe^{2+} ratios (Ballhaus et al., 1990, 1991). A pressure of 17 kbar was assumed for spinel lherzolites, whereas calculated pressures were used for garnet lherzolites. Temperatures in all cases were from the Ca-in-Opx thermometer. Results are listed in Table 8 as log unit deviations from the FMQ (fayalite–magnetite–quartz) buffer (O'Neill, 1987), and range from FMQ −2.62 to FMQ −0.13. There is a weak positive correlation between relative f_{O_2} value and Cr/(Cr + Al) of spinel within the lherzolite suite as a whole, corresponding to higher f_{O_2} for more refractory compositions (Ballhaus, 1993). The range for CPSL (ΔFMQ = −2.62 to −0.34) is larger than for SGL (ΔFMQ = −1.18 to −0.37). With one exception (ΔFMQ = −2.13 for the anomalously low-temperature XLT-5), the CRSL are restricted to the more oxidized values (ΔFMQ = −1.0 to −0.13).

Assuming the presence of C–O–H volatile components, almost all xenoliths are at or above the H_2O maximum defined by C–H_2O (Taylor and Green, 1987) so that the dominant C–O–H species would be H_2O and CO_2. However, hydrous phases are exceptionally rare in the Jetty Peninsula xenoliths, which may be due to the dominance of CO_2 in the more oxidized xenoliths (this is supported by the common occurrence of carbonates), but probably also to low H_2O activity in the more reduced ones. Graphite was identified in the Jetty Peninsula xenolith suite by Egorov and Andronikov (1989), although it was not found in the current sample set.

7.3. Mineral thermobarometry

7.3.1. The choice of thermobarometers

The evidence of textural and chemical disequilibrium in the SGL and MSL poses problems for temperature and pressure estimation, as thermobarometers assume equilibrium between coexisting phases. In their experimental calibration of thermobarometers for peridotites, Brey and Köhler (1990) recommended the following pairs of thermobarometers, noting that they best reproduced the experimental data:

(1) $T(2Px)_{BKN}$ (Opx–Cpx solvus thermometer) + P_{BKN} (Al-exchange between Opx and garnet);
(2) T_{Krogh} (Fe–Mg exchange between Cpx and garnet; Krogh, 1988) + P_{BKN};
(3) $T_{O'Neill}$ (Fe–Mg exchange between Ol and garnet; O'Neill and Wood, 1979) + P_{BKN};
(4) $T(2Px)_{BKN}$ + P_{KB} (Ca exchange between Ol and Cpx; Brey and Köhler, 1990).

All BKN thermobarometers are from Brey and Köhler (1990). The first three of these four are limited to garnet-bearing assemblages, and all have potential problems if one or more minerals (especially clinopyroxene) is not in equilibrium with other phases.

A later critical assessment by Xu et al. (1998) considered the applicability of various thermometers and barometers to peridotites and pyroxenites for deriving paleogeotherms from xenolith studies. They concluded that the best combinations for garnet-spinel lherzolites were (1) the $T(Ca\text{-in-Opx})_{BK}$ (Ca-in-Opx thermometer tentatively introduced by Brey and Köhler, 1990) with the Al-exchange between opx and garnet as calibrated by Nickel and Green (1985); and (2) $T(2Px)_{BKN}$ with P_{BKN} as recommended by Brey and Köhler (1990). For spinel lherzolites, they recommend either $T(Ca\text{-in-Opx})_{BK}$ or T_{SS} (the Al-exchange between opx and spinel; Sachtleben and Seck, 1981) as thermometers. They concluded that the earlier thermometers of Wells (1977) and Ellis and Green (1979) as well as the opx-garnet barometer of Wood (1974) are suitable only for pyroxenites with more Fe-rich compositions. Following O'Reilly et al. (1997), the use of the Ca-in-olivine barometer of Köhler and Brey (1990) was not recommended, as the errors were considered too large given uncertainties in the temperature determination.

For application to the Antarctic garnet- and garnet + spinel lherzolites, we need to consider the differences between these recommendations and the reasons for them, in addition to their specific applicability to the Jetty Peninsula samples. Temperatures and pressures have therefore been calculated using several thermometers and barometers for the Antarctic samples, and results are listed in Table 8. The crystals in the peridotites are generally uniform in composition, so that core compositions could be used for thermobarometry. This does not apply to kelyphites or to crystallized cpx in CRSL. All Jetty Peninsula samples are lherzolites with bulk rock Mg# of 86.8–91.2 (Table 3) and the lowest Mg# in primary olivine or pyroxene is 88.7, so that the recommendations of Brey and Köhler (1990) for peridotites with Mg# around 90 ought to be applicable. However, as we will see, this is not always true.

First, we note that the olivine–garnet thermometer of O'Neill and Wood (1979) was not considered by Xu et al. (1998) and the thermometer of Sachtleben and Seck (1981) was not tested by Brey and Köhler (1990). T_{Krogh} was eliminated by Xu et al. (1998), but on the basis that it was not suitable for pyroxenites, whereas Brey and Köhler (1990) recommended it for lherzolites. The Nickel and Green (1985) calibration is recommended by Xu et al., but was not favoured by Brey and Köhler. However, they rejected it on the basis that it did not reproduce experimental pressures in excess of 35 kbar well, but this is of no con-

Table 8
P–T conditions and oxygen fugacity values for Jetty Peninsula lherzolite xenoliths

Sample #	Rock type in combination with	Temperature (°C)							Pressure (kbar)					fO_2
		T(BKN) *P*(BKN)	*T*(Ca-Opx) *P*(NG)	*T*(Ca-Opx) 20 kbar	*T*(BKN)	*T*(Krogh) *P*(BKN)	*T* O'Neill *P*(BKN)	SS81	*P*(BKN) *T*(BKN)	*P*(NG) *T*(Ca-Opx)	*P*(BKN) *T*(O'Neill)	*P*(BKN) *T*(Krogh)	*P*(KB) *T*(Ca-Ol)	Δlog(FMQ) *T*(Ca-Opx)
U-16	SGL	1063	**1130**			1253	1353	1054	16.7	**21.0**	28.5	24.3		−1.03
U-17	SGL	1113	**1105**			1207	1161	1024	20.7	**21.7**	22.7	24.6		−1.18
U-47	SGL	1026	**1038**			1073	1076	1021	16.9	**19.8**	19.0	18.9		−0.81
U-3/3A	SGL	1219	**1182**			1314	1763	1111	22.9	**22.1**	45.6	26.6		−0.84
D-3	SGL	1189	**1127**			1358	1437	1106	21.5	**20.4**	31.4	28.2		−0.37
DK-8/3	SGL	1054	**1102**			1002	1081	1052	18.2	**21.9**	19.3	16.2		−1.11
D-N1	SGL	1157	**1136**			1284	1184	1123	19.4	**20.3**	20.5	24.5		−0.58
D-N4	SGL	1195	**1125**			1295	1243	1056	23.0	**21.5**	25.0	27.3		−1.06
XLT-1	SGL	1155	**1135**			1092	1673	1055	23.8	**23.7**	47.0	21.3		−0.66
3/1-3	SGL	1186	**1147**			1291	1302	1111	20.4	**20.4**	25.0	24.5		−0.71
15/1-2	SGL	1237	**1181**			1386	1470	1116	21.8	**20.9**	31.3	27.8		−0.80
U-1	CRSL			**1072**	1057			1043					10.9	−0.18
U-36	CRSL			**1104**	1137			1050					14.7	−0.13
U-N1	CRSL			**1091**	1049			1065					11.4	−1.00
U-4/9-2	CRSL			**1093**	1127			1069					15.6	−0.19
XLT-4	CRSL			**1101**	1070			1072					4.1	−0.13
XLT-5	CRSL			**834**	557			909					9.2	−2.13
U-3	CPSL			**1058**	1109			1001					8.8	−0.37
U-3/4-2	CPSL			**1033**	1011			986					13.5	−0.52
D-11	CPSL			**1028**	895			944					12.8	−2.62
D-24	CPSL			**1046**	955			934					12.7	−1.78
D-N2	CPSL			**1057**	963			990					12.3	−0.94
1/4-3	CPSL			**1035**	1041			980					19.6	−0.34
32601-9B	CPSL			**852**	88			851					33.7	−1.27
U-17-K	Kelyphite			**1285**										
D-N1-K	Kelyphite			**1336**										
XLT1-K	Kelyphite			**1303**										

Bold type are recommended thermometers and barometers for the Jetty Peninsula xenoliths (see text for discussion).
References for thermobarometers: Brey and Köhler (1990), BKN and Ca-in-Opx; Nickel and Green (1985), NG; Krogh (1988), Krogh; O'Neill and Wood (1979) and O'Neill; Sachtleben and Seck (1981), SS81. Oxygen fugacity calculated from Ballhaus et al. (1990) using temperature from Brey and Köhler's (1990) Ca-in-Opx thermometer.

cern to garnet + spinel lherzolites such as the Jetty Peninsula rocks.

Lherzolites containing both spinel and garnet present the best tests of thermobarometers. The combination of $T(2Px)_{BKN} + P_{BKN}$, recommended in both cited works, and the combination $T(Ca\text{-in-}Opx)_{BK} + P_{NG}$, recommended by Xu et al. (1998) yield largely similar results with realistic P–T values. In contrast, the thermometers of O'Neill and Wood (1979) and Krogh (1988) yield generally high temperatures, some erratically high, up to 1386 °C (Krogh, 1988) and in excess of 1700 °C (O'Neill and Wood, 1979; Table 8).

In application to garnet-free spinel lherzolites, the Ca-in-olivine barometer is the only available calibration, although it has been criticised by O'Reilly et al. (1997) as being more temperature- than pressure sensitive. Most results for the Jetty Peninsula spinel lherzolite xenoliths lie within the spinel lherzolite field (10.9–19.6 kbar), but they have large errors on the calculated pressure. The temperatures of all but the non-equilibrium spinel lherzolites fall within the narrow range of 1028–1104 °C, implying a much narrower pressure range than given by the Ca-in-olivine barometer. Furthermore, if the P–T pairs including the Ca-in-olivine barometer (which has an error of ±4 kbar; Köhler and Brey, 1990) are taken at face value, then an oversteep geothermal gradient much hotter than all those plotted in Fig. 9 results. Therefore, we plot the spinel lherzolites on a continuation of the geotherm defined by the SGL in Fig. 9, corresponding to a pressure range of 17–20.5 kbar.

Particularly erratic results either at apparent crustal pressures (4.1–9.2 kbar) or at >33 kbar are obtained for spinel lherzolites with low Ca contents in olivine. However, these spurious results are attributable to the lack of attainment of equilibrium between clinopyroxene and the earlier olivine and orthopyroxene and not to inaccuracy in the calibration; the approximate positions in Fig. 9 indicate that they plot well away from the main trend (thick solid line in Fig. 9).

The temperature calculated from Ca-in-Opx is a minimum estimate because it assumes equilibrium with clinopyroxene. In a study of spinel- and garnet-bearing peridotite xenoliths of the Vitim volcanic field in eastern Siberia, Glaser et al. (1999) noted that clinopyroxene grown later during rift-related metasomatism did not attain equilibrium with coexisting orthopyroxene, thus yielding invalid temperatures calculated from coexisting pyroxenes. However, as $T_{Ca\text{-in-}Opx}$ gives similar temperatures to the T_{BKN}–P_{BKN} pair, we consider these temperatures to be well-constrained for the Jetty Peninsula xenoliths. The T_{BKN} thermometer gives lower temperatures for many spinel lherzolites, whereby erratically low temperatures are returned for the low-Ca group (Table 8).

In conclusion, the pair $T(2Px)_{BKN} + P_{BKN}$ recommended by Brey and Köhler appear to provide consistently reliable results as long as clinopyroxene and orthopyroxene are in equilibrium: calculations based on their mere coexistence can lead to erroneous results. The second recommendation of Xu et al. ($T(Ca\text{-in-}Opx)_{BK} + P_{NG}$,) also gives reasonable results, and is preferred for the Jetty Peninsula SGL because it produces a discrete break between SGL and the spinel lherzolites. In the following comparison of xenoliths from different areas, we therefore use the recommendations of Xu et al. (1998) for spinel–garnet lherzolites. The thermometers of Brey and Köhler (1990; $T_{Ca\text{-in-}Opx}$) and Sachtleben and Seck (1981) both give reasonable results with no outliers for spinel lherzolites, except for the low-Ca group. For this group, the $T_{Ca\text{-in-}Opx}$ temperatures are taken as minimum estimates, whereas the pressures cannot be trusted.

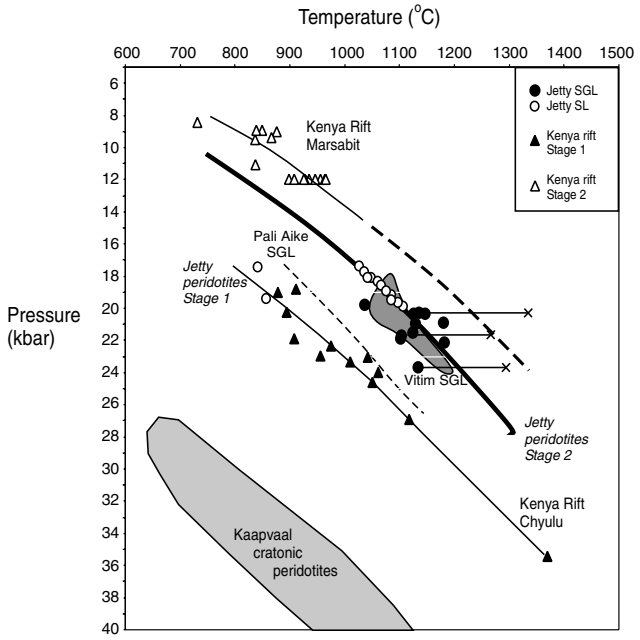

Fig. 9. Thermobarometry of Jetty Peninsula peridotites compared to other regions in rift settings or with garnet-bearing lherzolites. Data points for Jetty Peninsula are compared to geotherms for spinel–garnet lherzolites from Pali Aike (thin dotted line; Kempton et al., 1999a), and Vitim, Siberia (dark shaded area; Glaser et al., 1999), for two stages of the Kenya Rift (thin solid lines; Henjes-Kunst and Altherr, 1992), and Kaapvaal cratonic peridotites. The Jetty Peninsula main geotherm (thick solid line) is defined by the garnet-bearing samples; spinel lherzolites are fit to this geotherm based on the calculated temperatures (see text). The two low temperature exceptions are low-CaO rocks and are attributed to harzburgitic protoliths and a lack of equilibrium of clinopyroxene with olivine and orthopyroxene. Crosses indicate temperatures from kelyhite rim assemblages connected to the main mineral population of the same rocks by a solid line, assuming no change in pressure. The Jetty rocks contain information on three stages of rift development; the first, coldest stage is recorded only in the low-CaO spinel lherzolites, the second stage by the main population, and the third by the kelyphite rims. The first and third stages are very similar to those defined for the East African rift, whereby the kelyphites fit on a deeper extension of the Marsabit geotherm (thick dotted line).

7.3.2. Fossil geotherms in the Lambert–Amery Rift

The pressure–temperature calculations for the Jetty Peninsula xenoliths are plotted in Fig. 9 together with xenolith data for Pali Aike, Chile (Kempton et al., 1999a), Vitim, Siberia (Ionov et al., 1993; Glaser et al., 1999; Litasov

et al., 2000) and from the East African Rift (Henjes-Kunst and Altherr, 1992). The pressures and temperatures are well-determined for the garnet + spinel lherzolites, and the pressure range of 19.8–23.7 kbar (Table 8; Fig. 10) compares favourably with 17.4–21.7 kbar for Nushan (Xu et al., 1998), 18.2–23.1 kbar for Pali Aike (Kempton et al., 1999a) and 18.1–23.8 kbar for Vitim (Ionov et al., 1993). The temperatures for the spinel lherzolites are fit to the geotherm defined by the garnet-bearing samples, resulting in a much tighter pressure range (17–20.5 kbar) for the spinel lherzolites than calculated with the P_{KB} barometer, which would result in a subvertical geotherm. The temperatures for high-Ca xenoliths show a general increase in the order CPSL (1028–1058 °C) through CRSL (1072–1104 °C) to SGL (1102–1181 °C, except one value of 1038 °C) in keeping with a deeper position on a geotherm for the garnet-bearing samples.

The comparison in Fig. 9 shows that evidence for three temporally separated geotherms survive in the Jetty Peninsula xenolith record. The bulk of data points lie on a geotherm similar to the higher temperature samples from Vitim. The two open circles are low-Ca spinel lherzolites with temperatures of 830–910 °C by both the Ca-in-Opx and Sachtleben and Seck (1981) thermometers. Application of the P_{KB} barometer for the low-Ca group results in highly erratic pressures (4–34 kbar) which can be explained by the lack of equilibrium between olivine and clinopyroxene. As orthopyroxene CaO contents are also low (2170–4160 vs. 6900–9600 ppm for the high-Ca group), these samples appear to be derived from a low temperature harzburgitic protolith. Assuming that they originate from the same 17–20 kbar range, the low-Ca xenoliths lie approximately on the geotherm of Chyulu, Kenya, which is also a rift-related early stage geotherm (Henjes-Kunst and Altherr, 1992).

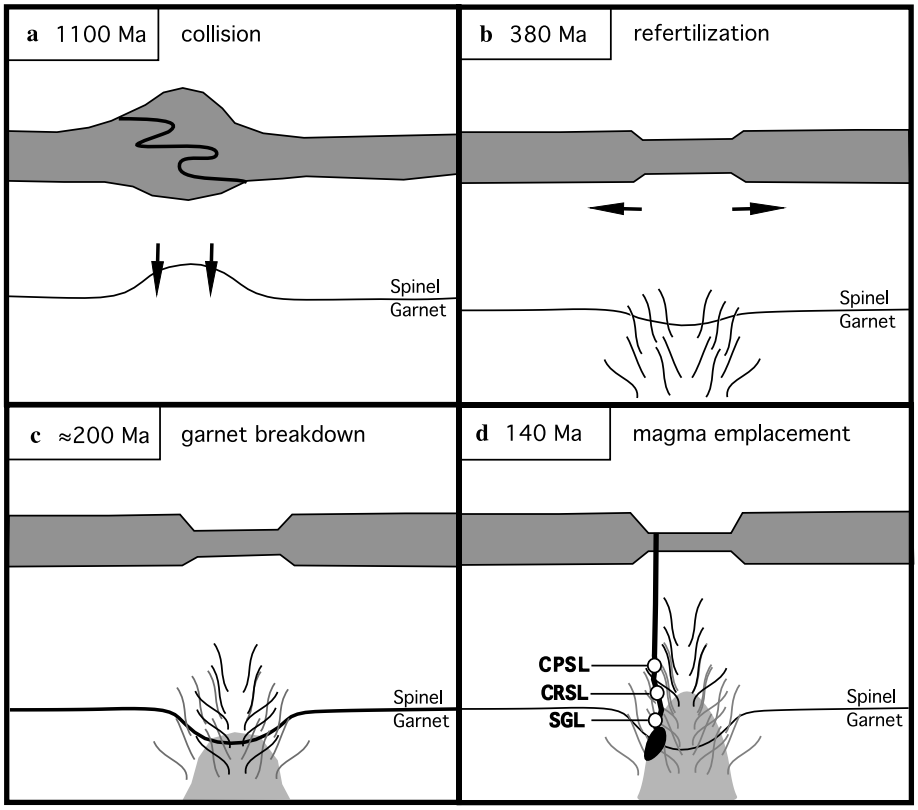

Fig. 10. Schematic tectonic history of mantle events in the Lambert-Amery Rift region. The low-Ca harzburgitic protoliths predate events illustrated here, and may date back to the late Archaean. (a) Collision at 1100 Ma caused crustal thickening and downwarping of the underlying mantle. Removal of cooler upper mantle to deeper levels (arrows) resulted in growth of garnet in lherzolites previously in the spinel field. (b) The first signs of rifting, dated at 375–390 Ma by clinopyroxene ages (Andronikov and Beliatsky, 1995) correspond to infiltration of peridotites by melts and growth of clinopyroxene. Veining beneath the central parts of the incipient rift is caused by melting at deeper levels than illustrated here. (c) Further evolution of the rift results in movement of both partial melting (grey field) and veining to higher levels. Accentuated heating in the central region beneath the rift causes the spinel–garnet peridotite boundary to warp downwards to higher pressures, so that garnets break down to form kelyphites. The age corresponding to panel (c) is only approximate, but textural evidence shows that kelyphite formation must appreciably predate magma emplacement. Further evolution of the rift (d) results in veining and melting at higher levels, including the generation of ultramafic lamprophyre melts which host the peridotite xenolith suite. The open circles show the regions of origin of the three xenolith classes: SGL are derived from depths previously in the garnet stability field, but now in the spinel field since sub-rift heating occurred; CRSL are derived from levels above the earlier spinel–garnet boundary that experienced thorough re-enrichment by rift-related melt infiltration. CPSL retain chemical signals from the time before rifting events started, and have avoided extensive enrichment in clinopyroxene either due to being at higher levels, or üerhaps to being situated between melt pathways in (b) and (c).

Although the Ca-in-Opx thermometer assumes equilibrium with clinopyroxene, it can be used as a minimum estimate where only an analysis of Ca in orthopyroxene is available. Application of this technique to orthopyroxene within kelyphite rims around garnet in the SGL gives temperatures 180–200 °C higher than the main orthoyproxene population within the same rocks. These temperatures resemble the extension of the high-temperature Marsabit geotherm from the Kenya Rift (thick dotted line in Fig. 9), again linking the temperature information of the Jetty Peninsula to the evolution of the mantle beneath a developing rift.

7.4. Cold harzburgite protoliths

Several lines of evidence indicate that many protoliths of Jetty Peninsula peridotite xenoliths were harzburgites derived from colder conditions than indicated by the main geotherm in Fig. 9. The anomalous thermobarometric results (vestigial low temperatures of 835-910 °C) for CPSL sample 32601-9B and CRSL sample XLT-5 are caused by a lack of equilibrium of clinopyroxene with olivine coupled with low concentrations of calcium in the olivine (<300 ppm) and orthopyroxene (<4600 ppm; Table 7). The low-Ca contents are accompanied by lower contents of Ti, V, Cr and Zn in both olivine and orthopyroxene and additionally low Cu, Ni, Ga and Li in orthopyroxenes relative to these minerals in other samples (Figs. 7 and 8). The lack of intermineral trace element equilibrium in samples of the low-Ca group is underlined by fact that the whole-rock concentrations of CaO are not lower than in other samples. Sample XLT-4 also belongs to the low-Ca group although it does not return anomalously low temperatures (the Ca-in-olivine barometer gives 4 kbar). Although none of the spinel–garnet lherzolites were found to belong to the low-Ca group as defined above by olivine and orthoyproxene trace element chemistry, two samples (U3/3A and XLT-1) contain subcalcic garnets, showing that they originally grew in a clinopyroxene-free rock. This observation indicates that garnet is able to preserve information of protoliths longer than olivine and orthopyroxene, which is in keeping with slower divalent cation diffusivities in garnet.

Taken together, these characteristics argue for the widespread occurrence of depleted peridotites at some time prior to development of the rift. Furthermore, they indicate that even the low modal clinopyroxene (average 5%) in the CPSL was introduced at a later stage, and the higher modal clinopyroxene in CRSL and SGL groups may indicate more than one episode of refertilization (clinopyroxene growth). Later refertilization of depleted mantle peridotites is increasingly recognised in both cratonic (Simon et al., 2003) and non-cratonic (Glaser et al., 1999) areas.

7.5. The possible relation of fossil geotherms to tectonic events

The thermobarometric results given in Table 8 and Fig. 9 indicate that spinel lherzolites equilibrated at lower temperatures than spinel + garnet lherzolites. The clinopyroxene-poor spinel lherzolites are the most geochemically depleted group (Fig. 4) and appear to represent the uppermost levels of the mantle beneath the margins of the Lambert–Amery Rift. Clinopyroxenes from both CRSL and SGL are overprinted with secondary rims and their whole-rock compositions are less depleted than the CPSL (Fig. 4). The SGL appear to be compositionally homogeneous, whereas the CRSL are more variable and show more scatter on Figs. 3–6. The depletion of the uppermost mantle lithosphere (CPSL) corresponds to the expected vertical zonation that results from partial melting beneath a mid-ocean ridge (Langmuir et al., 1992).

It can be argued on the basis of the exceptionally low-Ca contents in olivine and orthoyproxene (Table 7; Figs. 7,8) that the low temperature signature of the two anomalous samples applies to previously existing harzburgites which were later refertilized. However, assuming these samples were at all times at depths corresponding to spinel lherzolite stability, even this colder geotherm (>60 mWm^{-2}) is well above typical cratonic geotherms (ca. 45 mWm^{-2}; Brey and Köhler, 1990), meaning that no evidence for a cratonic geotherm is preserved beneath the southern Prince Charles Mountains (Fig. 1). The interpretation of earlier, colder conditions in harzburgitic protoliths also implies that refertilization affected all peridotite groups, accounting for the widespread presence of clinopyroxene. The interpretation of anomalous barometric results for the low-Ca group as erroneous due to lack of intermineral equilibrium eliminates the necessity that these samples originate from greatly different depths from all the others.

Most samples from all three Jetty Peninsula lherzolite groups appear to fall on a geotherm intermediate between the early and late stages of the Kenya Rift, and slightly higher than the geotherms corresponding to the Pali Aike and Vitim rocks (Fig. 9). This observation indicates a thorough heating of the mantle beneath the rift; although the timing cannot be precisely determined, it must have occurred shortly before sampling by the host magma in order to allow preservation of the earlier chemical signal and of textural evidence for the earlier episodes.

A later event is indicated by the kelyphite rims. An indication of the thermal deviation of this event from pre-existing conditions can be gained from Ca-in-orthopyroxene thermometry of secondary minerals in the kelyphite rims. These give temperatures of 1285–1336 °C, corresponding to 180–200 °C higher than for primary orthopyroxenes in the SGL. This temperature increase corresponds to that seen in the Kenya Rift (Fig. 10b) and can also account for the clinopyroxene rims whose chemistry is best explained by incipient melting. The presence of rim structures and kelyphite aggregates in lherzolite xenoliths has been reported for various rift-related regions (Frey and Green, 1974; Henjes-Kunst and Altherr, 1992), and these structures are mainly interpreted as generated during ascent of the xenoliths to the surface, or to upwelling of mantle domains. However, the com-

plete lack of clinopyroxene rim formation in the CPSL is difficult to explain if the rims originate purely by heating in the host magma: the CPSL average only 50 °C cooler than the CRSL, so that partial melting of rims in one case and the complete lack of any textural effect in the other appears to be inconsistent. The solution to this apparent dilemma is not clear, but it may be that the CRSL correspond to the uppermost level that was affected by the upward and outward migration of heating due to the progressive extension of the rift. It may be that clinopyroxene rim formation could develop only in rocks where an intergranular melt was already present at the extremities of rift metasomatism, thus causally linking the production of clinopyroxene to metasomatism by fluxing of the incipient melting.

In summary, there are rare indications for a colder continental geotherm (≈60 mWm^{-2}) which pre-dated the main xenolith geotherm. This interpretation is consistent with emplacement of metasomatic melts from below, as the CPSL xenoliths in the upper levels of the lithosphere were not affected. The formation of recrystallized and partially melted rims of clinopyroxene and garnet is younger, but preceded the emplacement in the host magma, and was fluxed by migration of metasomatic melts related to the development of the rift.

7.6. Sequence of events and their relation to the Lambert–Amery Rift

Despite the rarity of outcrops, we can be fairly certain that the Jetty Peninsula area is underlain by continental crust of mid-Proterozoic age. Archean rocks are present to the south and east (Fig. 1), but are not known within 200 km of the study area. The earliest magmatic activity dates from 320 Ma, when doleritic to lamprophyric dykes were emplaced in the Jetty Peninsula area (Mikhalsky and Sheraton, 1993). Later magmatism between 150 and 140 Ma resulted in the emplacement of the peridotite xenolith suite.

The history of the Jetty Peninsula xenoliths before entrainment in the host magma can be summarized in four periods recognisable from evidence in the xenoliths. The first is recorded by the sub-900 °C temperatures in the CPSL, and may correspond to the 2.6 Ga Sm–Nd age of Mukasa and Andronikov (1999). These samples indicate a colder palaeogeotherm than the main xenolith population, and this colder geotherm corresponds to the harzburgitic protoliths before re-enrichment and the (re-) introduction of clinopyroxene. These were refertilized at later stage as gauged by the occurrence of about 5% clinopyroxene, but the timing of the refertilization, which probably affected all xenolith groups, remains uncertain. A second event caused the formation of garnet from spinel in the SGL: we suggest that this event results from a pressure increase during collision (Fig. 10a), which may be linked to the time of widespread reconstruction of the lithosphere and new crust generation during the collision between Antarctic and Indian Shields at ca. 1.1 Ga (Sheraton et al., 1993; Andronikov and Beliatsky, 1996).

Subsequent events are all related to the initiation and development of the Lambert–Amery Rift. As the rift develops, the effective lithosphere-asthenosphere boundary moves upwards and outwards as the upward movement of hotter asthenosphere heats its surroundings (Fig. 10b). This may lead to the generation of partial melts that move upwards and metasomatize the lower lithosphere (Glaser et al., 1999). These low volume melts modified the SGL and CRSL, but did not reach the CPSL. This may be because the CPSL lie at higher levels in the lithosphere (the lower temperature is a better gauge for this than the pressures, which have a larger uncertainty), but may also be a localized effect caused by the CRSL being close to veins formed from melt infiltration, whereas the CPSL lay further away from the veins. This period of melt infiltration and chemical re-enrichment may be associated with the beginning of intensive tholeiite dyke magmatism (320 Ma; Mikhalsky and Sheraton, 1993) and so may mark the earliest datable constraint for rifting. It probably also corresponds to the clinopyroxene ages of 374 Ma (Andronikov and Beliatsky, 1995) and 390 Ma for the CRSL (Mukasa and Andronikov, 1999). Nevertheless, the presence of 15% clinopyroxene in some samples that earlier were demonstrably harzburgites argues for multiple enrichment episodes which were probably not restricted to the times illustrated in Fig. 10.

Foley et al. (2002) proposed a model of veining of the mantle beneath this area to explain the genesis of ultramafic lamprophyres emplaced at 115 Ma. These rocks show an array of isotopic signatures with variable $^{87}Sr/^{86}Sr$ but constant $^{143}Nd/^{144}Nd$, which can be explained by growth of $^{87}Sr/^{86}Sr$ from phlogopite located in veins which were themselves formed 150–200 Ma earlier, whereas the 200 Ma time period is insufficient to allow a measureable change of Nd isotopes. The time needed to explain the $^{87}Sr/^{86}Sr$ signature in the ultramafic lamprophyres corresponds to the difference between the age of the lamprophyres (115 Ma) and the enrichment event seen in the clinopyroxenes (374–390 Ma). We surmise that the period of veining activity was associated with an episode of subrift asthenospheric expansion at 375–390 Ma, and this probably corresponds to that of the main Jetty Peninsula geotherm (Fig. 9). The main geothermal conditions indicated in Fig. 9 are characteristic for hot, shallow lithospheric mantle either in rift-related regions (Berg et al., 1989; Henjes-Kunst and Altherr, 1992) or related to magmatic activity within the mantle as evidenced by pyroxenite veins (Xu et al., 1996; Litasov et al., 2000).

Further heating occurred in the lower lithosphere as rifting progressed, so that the spinel–garnet transition moved gradually to higher pressures, passing the position of the SGL, and resulting in the breakdown of garnet to form the kelyphites (stage 4; Fig. 10c). This strong heating event was not associated with influx of water, as indicated by the dry breakdown reaction in the kelyphite

rims, and resulted also in the formation of rims on clinopyroxene. Stage 4 must have occurred within 2 Ma before emplacement, as constrained by the necessity to preserve the non-equilibrium textures of rims to clinopyroxene, spinel and garnet (Glaser et al., 1999). The examples of grain-coarsening in kelyphitic material noted above further indicate that an appreciable period of time must have passed between kelyphite formation and xenolith emplacement. Finally, during or immediately before the incorporation of the xenoliths into the host magma (Fig. 10d), infiltration of melt into the rocks occurred, which is recorded by the glassy margins around spinels and as rare interstitial melt pools. The association of these glasses with the host magma is indicated by their higher alkali contents.

Acknowledgments

This investigation was financially supported by a Alexander von Humboldt-Stiftung fellowship for A.V.A. and by the Deutsche Forschungsgemeinschaft's Gerhard Hess Programm to S.F.F. The authors are grateful to E.V. Mikhalsky and A.A. Laiba for allowing use of part of their xenolith collections in this study. The manuscript has benefitted from comments by C-.T. Lee, T. Furman, S. O'Reilly, I. Parkinson, M. Bizimis and P. Kempton. SFF thanks T. Köhler for advice on thermobarometry. This is Mainz Geocycles Cluster contribution No. 10.

Associate editor: Martin A. Menzies

References

Andersen, T., Griffin, W.L., O'Reilly, S.Y., 1987. Primary sulphide melt inclusions in mantle-derived magacrysts and pyroxenites. *Lithos* **20**, 279–294.

Andrews, J.R., Emeleus, C.H., 1976. Kimberlites of West Greenland. In: Escher, A., Watt, W.S. (Eds.), *Geology of Greenland*. Geological Survey of Greenland, Copenhagen, pp. 575–589.

Andronikov, A.V., 1990. Spinel–garnet lherzolite nodules from alkaline-ultrabasic rocks of Jetty Peninsula (East Antarctica). *Antarct. Sci.* **2**, 321–330.

Andronikov, A.V., 1997. Varying glass compositions in deep-seated inclusions from alkaline–ultramafic rocks of Jetty Peninsula (East Antarctica): evidence for mantle metasomatism. In: Ricci, C.A. (Ed.), *The Antarctic Region: Geological Evolution and Processes*. University of Siena, pp. 901–910.

Andronikov, A.V., Beliatsky, B.V., 1995. Implication of Sm–Nd isotopic systematics to the events recorded in the mantle-derived xenoliths from the Jetty Peninsula, East Antarctica. *Terra Antarct.* **2**, 103–110.

Andronikov A.V., Beliatsky B.V., 1996. Manning Massif alkaline trachybasalts (MAT): some characteristics of enriched lithospheric mantle source. In: *Proceedings Seventh Freiberg Isotopic Collquium*, Freiberg, pp. 9–18.

Andronikov, A.V., Egorov, L.S., 1993. Mesozoic alkaline–ultramafic magmatism of Jetty Peninsula. In: Findlay, R.H., Unrug, R., Banks, M.R., Veevers, J.J. (Eds.), *Gondwana Eight: Assembly, Evolution and Dispersal*. Balkema, Rotterdam, Brookfield, pp. 547–557.

Andronikov, A.V., Mikhalsky, E.V., 1997. Deep-seated xenoliths from Proterozoic ultramafic lamprophyre dykes of the Vestfold Hills (East Antarctica): evidence for the existence of metasomatized lithosphere. In: Ricci, C.A. (Ed.), *The Antarctic Region: Geological Evolution and Processes*. University of Siena, pp. 911–921.

Andronikov, A.V., Mikhalsky, E.V., Beliatsky, B.V., 1994. Abyssal xenoliths from the lamprophyres of the Vestfold Hills, East Antarctica. *Petrology* **2**, 250–257.

Ashchepkov, I.V., Litasov, Y.D., Dobretsov, N.L., 1994. Pyroxenites and composite garnet peridotite xenoliths from picrite-basalt, Vitim plateau (Trans-Baikal): implications for thermobarometry and mantle reconstruction. In: Meyer, H.O.A., Leonardos, O.H. (Eds.), *Kimberlites, Related Rocks and Mantle Xenoliths*. C.P.R.M. Special Publ. 1/A, Brasilia, pp. 455–466.

Ballhaus, C., 1993. Redox states of lithospheric and asthenospheric upper mantle. *Contrib. Mineral. Petrol* **114**, 331–348.

Ballhaus, C., Berry, R.F., Green, D.H., 1990. Oxygen fugacity controls in the Earth's upper mantle. *Nature* **348**, 437–440.

Ballhaus, C., Berry, R.F., Green, D.H., 1991. High pressure experimental calibration of the olivine–orthopyroxene–spinel oxygen barometer: implications for the oxidation state of the upper mantle. *Contrib. Mineral. Petrol* **107**, 27–40.

Berg, J., Mascati, R., Herz, D., 1989. A petrologic geotherm from a continental rift in Antarctica. *Earth Planet. Sci. Lett.* **93**, 98–108.

Bernstein, S., Kelemen, P.B., Brooks, C.K., 1998. Depleted spinel harzburgite xenoliths in Tertiary dykes from East Greenland: Restites from high degree melting. *Earth Planet. Sci. Lett.* **154**, 221–235.

Bizzarro, M., Stevenson, R., 2003. Major element composition of the lithospheric mantle under the North Atlantic craton: evidence from peridotite xenoliths of the Sarfartoq area, southwestern Greenland. *Contrib. Mineral. Petrol.* **146**, 223–240.

Bottazzi, P., Tiepolo, M., Vannucci, R., Zanetti, A., Foley, S., Brumm, R., Oberti, R., 1999. Distinct site preferences for heavy and light rare-earth elements and the prediction of $^{Amph/L}D_{REE}$. *Contrib. Mineral. Petrol.* **137**, 36–45.

Boyd, F.R., 1989. Compositional distinction between oceanic and cratonic lithosphere. *Earth Planet. Sci. Lett.* **96**, 15–26.

Boyd, F.R., Mertzmann, S., 1987. Composition and structure of the Kaapvaal lithosphere, Southern Africa. In: Mysen, B.O. (Ed.), *Magmatic Processes: Physicochemical Principles*, vol. 1. Geochemical Society Spec. Publ, pp. 13–24.

Boyd, F.R., Pokhilenko, N.P., Pearson, D.G., Mertzman, S.A., Sobolev, N.V., Finger, L.W., 1997. Composition of the Siberian cratonic mantle: evidence from Udachnaya peridotite xenoliths. *Contrib. Mineral. Petrol.* **128**, 228–246.

Brey, G.P., Köhler, T., 1990. Geothermobarometry in four-phase lherzolites II. New thermobarometers, and practical assessment of existing thermobarometers. *J. Petrol.* **31**, 1353–1378.

Bulatov, V., Brey, G.P. Foley, S.F., 1991. Origin of low-Ca, high-Cr garnets by recrystallization of low-pressure harzburgites. *Ext. Abs. 5th Int Kimberlite Conf, Araxá*, C.P.R.M. Special Publ. 2/91. Brasilia, pp. 29–31.

Chalmers, J.A., Laursen, K.H., 1995. Labrador sea: the extent of continental and oceanic crust and the timing of the onset of sea-floor spreading. *Mar. Petrol. Geol.* **12**, 205–217.

Chazot, G., Menzies, M., Harte, B., 1996a. Silicate glasses in spinel lherzolites from Yemen: origin and chemical composition. *Chem. Geol.* **134**, 159–179.

Chazot, G., Menzies, M., Harte, B., 1996b. Determination of partition coefficients between apatite, clinopyroxene, amphibole and melt in natural spinel lherzolites from Yemen: implications for wet melting of the lithospheric mantle. *Geochim. Cosmochim. Acta* **60**, 423–437.

Dawson, J.B., 1980. *Kimberlites and Their Xenoliths*. Springer-Verlag, Berlin, p. 252.

Delaney, J.S., Smith, J.V., Nixon, P.H., 1979. Model for upper mantle below Malaita, Solomon Islands, deduced from chemistry of lherzolite and megacryst minerals. *Contrib. Mineral. Petrol.* **70**, 209–218.

Drury, M.R., FitzGerald, J.D., 1996. Grain boundary melt films in an experimentally deformed olivine–orthopyroxene rock: implications for melt distribution in upper mantle rocks. *Geophys. Res. Lett.* **23**, 701–704.

Egorov, L.S., Andronikov, A.V., 1989. New data on stock bodies of alkaline-ultrabasic rocks of Jetty Peninsula (McRobertson Land, East Antarctica) obtained during the 1986/1987 season. *Inf. Bull. SAE* **111**, 5–13 (in Russian).

Ehrenberg, S.N., 1982. Petrogenesis of garnet lherzolite and megacrystalline nodules from the Thumb, Navajo volcanic field. *J. Petrol.* **23**, 507–547.

Ellis, D.J., Green, D.H., 1979. An experimental study of the effect of Ca upon garnet–clinopyroxene Fe–Mg exchange equilibria. *Contrib. Mineral. Petrol.* **71**, 13–22.

Emeleus, C.H., Andrews, J.R., 1975. Mineralogy and petrology of kimberlite dyke and sheet intrusions and included peridotite xenoliths from south-west Greenland. *Phys. Chem. Earth* **9**, 179–197.

Falloon, T.J., Green, D.H., Danyushevsky, L.V., Faul, U.H., 1999. Peridotite melting at 1.0 and 1.5 GPa: an experimental evaluation of techniques using diamond aggregates and mineral mixes for determination of near-solidus melts. *J. Petrol.* **40**, 1343–1375.

Fan, Q., Hooper, P.R., 1989. The mineral chemistry of ultramafic xenoliths of eastern China: implications for upper mantle composition and the paleogeotherms. *J. Petrol.* **30**, 1117–1158.

Foley, S.F., Andronikov, A.V., Melzer, S., 2002. Petrology, geochemistry and mineral chemistry of ultramafic lamprophyres from the Jetty Peninsula area of the Lambert-Amery Rift, Eastern Antarctica. *Mineral. Petrol.* **74**, 361–384.

Franz, L., Wirth, R., 1997. Thin intergranular melt films and melt pockets in spinel peridotite xenoliths from the Rhön area (Germany): early stage of melt generation by grain boundary melting. *Contrib. Mineral. Petrol.* **129**, 268–283.

Frey, F.A., Green, D.H., 1974. The mineralogy, geochemistry and origin of lherzolite inclusions in Victorian basanites. *Geochim. Cosmochim. Acta* **38**, 1023–1059.

Frey, F.A., Prinz, M., 1978. Ultramafic inclusions from San Carlos, Arizona: petrologic and geochemical data bearing on their petrogenesis. *Earth Planet. Sci. Lett.* **38**, 129–176.

Garvie, O.G., Robinson, D.N., 1982. The mineralogy, structure and mode of formation of kelyphite and associated sub-kelyphitic surfaces on pyrope from kimberlite. *Terra Cognita* **2**, 229–230.

Glaser, S.M., Foley, S.F., Günther, D., 1999. Trace element compositions of minerals in garnet and spinel peridotite xenoliths from the Vitim volcanic field, Transbaikalia, eastern Siberia. *Lithos* **48**, 263–285.

Grikurov, G.E., Orlenko, E.M., Fedorov, L.V., 1980. Alkaline-ultrabasic rocks of the Beaver Lake region, East Antarctica. *Tr. Sov. Antarct. Exped.* **70**, 87–99 (in Russian).

Harte, B., 1983. Mantle peridotites and processes—the kimberlite sample. In: Hawkesworth, C.J., Norry, M.J. (Eds.), *Continental Basalts and Mantle Xenoliths*. Shiva, Nantwich, pp. 46–91.

Harte, B., Hunter, R.H., Kinny, P.D., 1993. Melt geometry, movement and crystallization, in relation to mantle dykes, veins and metasomatism. *Philos. Trans. R. Soc. Lond. A* **342**, 1–21.

Henjes-Kunst, F., Altherr, R., 1992. Metamorphic petrology of xenoliths from Kenya and Northern Tanzania and implications for geotherms and lithopsheric structures. *J. Petrol.* **33**, 1125–1156.

Hunter, R.H., Taylor, L.A., 1982. Stability of garnet from the mantle: glass as evidence of metasomatic melting. *Geology* **10**, 617–620.

Ionov, D.A., Ashchepkov, I.V., Stosch, H.G., Witt-Eickschen, G., Seck, H.A., 1993. Garnet peridotite xenoliths from the Vitim volcanic field, Baikal region: the nature of the garnet–spinel peridotite transition zone in the continental mantle. *J. Petrol.* **34**, 1141–1175.

Jacob, D.E., 2006. Trace and ultra-trace element analysis of geological reference materials by Laser-ablation inductively coupled plasma mass spectrometry (LA-ICP-MS). *Geostand. Geoanal. Res.* (in press).

Jacob, D.E., Jagoutz, E., Sobolev, N.V., 1997. Neodymium and strontium isotopic measurements on single subcalcic garnet grains from Yakutian kimberlites. *N. Jb. Min. Abh.* **172**, 357–379.

Kempton, P.D., Lopez-Escobar, L., Hawkesworth, C.J., Pearson, D.G., Wright, D.W., Ware, A.J., 1999a. Spinel ± garnet lherzolite xenoliths from Pali Aike, Part 1: Petrography, mineral chemistry and geothermobarometry. In: Dawson, J.B., Gurney, J.J., Gurney, J.L., Pascoe, M.D. Richardson, S.H. (Eds.), *Proceedings of the Seventh International Kimberlite Conference*. Red Roof, Cape Town, pp. 403–414.

Kempton, P.D., Hawkesworth, C.J., Lopez-Escobar, L., Pearson, D.G., Ware, A.J., 1999b. Spinel ± garnet lherzolite xenoliths from Pali Aike, Part 2: Trace element and isotopic evidence bearing on the evolution of lithospheric mantle beneath southern Patagonia. In: Dawson, J.B., Gurney, J.J., Gurney, J.L., Pascoe, M.D., Richardson, S.H. (Eds.), Proceedings of the Seventh International Kimberlite Conference. Red Roof, Cape Town, pp. 415–428.

Klemme, S., 2002. The influence of Cr on the garnet–spinel transition in the Earth's mantle: experiments in the system MgO–Cr_2O_3–SiO_2 and thermodynamic modelling. *Lithos* **77**, 639–646.

Köhler, T., Brey, G.P., 1990. Ca-exchange between olivine and clinopyroxene as a geothermobarometer calibrated from 2 to 60 kbar in primitive natural lherzolites. *Geochim. Cosmochim. Acta* **54**, 2375–2388.

Kovach, V.P., Beliatsky, B.V., 1991. Geochemistry and age of granitic rocks in the Rucker granite–greenstone terrain, southern Prince Charles Mountains, East Antarctica. *Abs. VI Int. Symp. Antarctic Earth Sci.*, Tokyo, pp. 321–326.

Krogh, E.J., 1988. The garnet–clinopyroxene Fe–Mg–geothermometer—a reinterpretation of existing experimental data. *Contrib. Mineral. Petrol.* **99**, 44–48.

Kurinin, R.G., Grikurov, G.E., 1980. Structure of the Lamber Glacier rift zone. *Tr. Sov. Antarct. Exped.* **70**, 75–86 (in Russian).

Laiba, A.A., Andronikov, A.V., Egorov, L.S., Fedorov, L.V., 1987. Stock-like and dyke bodies of alkaline–ultrabasic composition in Jetty Peninsula (Prince Charles Mountains, East Antarctica). In: Grikurov, G.E., Ivanov, I.L. (Eds.), *Geologic and Geophysic investigations in Antarctica*. Leningrad, Sevmorgeologia, pp. 35–47 (in Russian).

Lee, C.T., Rudnick, R.L., Brimhall, G.H., 2001. Deep liothospheric dynamics beneath the Sierra nevada during the Mesozoic and Cenozoic as inferred from xenolith petrology. Geochem. Geophys, Geosyst. vol. 2, Paper No. 2001GC000152.

Langmuir, C.H., Klein, E.M., Plank, T., 1992. Petrological systematics of mid-ocean ridge basalts: constraints on melt generation beneath ocean ridges. In: Phipps Morgan, J., Blackman, D.K., Sinton, J.M. (Eds.), *Mantle Flow and Melt Generation at Mid-ocean Ridges*, vol. 71. AGU Monographs, pp. 183–280.

Litasov, K.D., Foley, S.F., Litasov, Y.D., 2000. Magmatic modification and metasomatism of the subcontinental mantle beneath the Vitim volcanic field (East Siberia): evidence from trace element data on pyroxenite and peridotite xenoliths from Miocene picrobasalt. *Lithos* **54**, 83–113.

Marks, M., Halama, R., Wenzel, T., Markl, G., 2004. Trace element variations in clinopyroxene and amphibole from alkaline to peralkaline syenites and granites: implications for mineral-melt trace-element partitioning. *Chem. Geol.* **211**, 185–215.

McDonough, W.F., Rudnick, R.L., 1998. Mineralogy and composition of the upper mantle. *Rev. Mineral.* **37**, 139–164.

McDonough, W.F., Sun, S.S., 1995. The composition of the earth. *Chem. Geol.* **120**, 223–253.

Mechie, J., Keller, G.R., Prodehl, C., Khan, M.A., Gaciri, S.J., 1997. A model for the structure, composition and evolution of the Kenya rift. *Tectonophysics* **278**, 95–119.

Menzies, M.A., 1983. Mantle ultramafic xenoliths in alkaline magmas: evidence for mantle heterogeneity modified by magmatic activity. In: Hawkesworth, C.J., Norry, M.J. (Eds.), *Continental Basalts and Mantle Xenoliths*. Shiva, Nantwich, pp. 92–110.

Mikhalsky, E.V., Sheraton, J.W., 1993. Association of dolerite and lamprophyre dykes, Jetty Peninsula (Prince Charles Mountains, East Antarctica). *Antarct. Sci.* **5**, 297–307.

Mukasa, S.B., Andronikov, A.V., 1999. Trace element and Sm–Nd and Rb–Sr isotopic evidence for the incipient melting of clinopyroxene in lherzolite xenoliths of the Jetty Peninsula area, East Antarctica. *EOS, Trans. Am. Geophys. Union* **80**, S379.

Nickel, K.G., Green, D.H., 1985. Empirical geothermobarometry for garnet peridotites and implications for the nature of the lithosphere, kimberlites and diamonds. *Earth Planet. Sci. Lett.* **73**, 158–170.

Nixon, P.H., Coleman, P.J., 1978. Garnet-bearing lherzolites and discrete nodule suites from the Malaita alnöite, Solomon Islands, and their bearing on the nature and origin of the Ontong Java Plateau. *Bull. Aust. Soc. Explor. Geophys.* **9**, 103–107.

Nixon, P.H., Rogers, N.W., Gibson, I.L., Grey, A., 1981. Depleted and fertile mantle xenoliths from southern African kimberlites. *Ann. Rev. Earth Planet. Sci.* **9**, 285–309.

O'Neill, H.S., 1981. The transition between spinel lherzolite and garnet lherzolite, and its use as a geobarometer. *Contrib. Mineral. Petrol.* **77**, 185–194.

O'Neill, H.S., 1987. The quartz–fayalite–iron and quartz–fayalite–magnetite equilibria and the free energies of formation of fayalite (Fe_2SiO_4) and magnetite (Fe_3O_4). *Am. Mineral.* **72**, 67–75.

O'Neill, H.S., Wood, B.J., 1979. An experimental study of Fe–Mg partitioning between garnet and olivine and its calibration as a geothermometer. *Contrib. Mineral. Petrol.* **70**, 59–70.

O'Reilly, S.Y., Chen, D., Griffin, W.L., Ryan, C.G., 1997. Minor elements in olivine from spinel lherzolite xenoliths: implications for thermobarometry. *Mineral. Mag.* **61**, 257–269.

Pearce, N.J.G., Perkins, W.T., Westgate, J.A., Gorton, M.P., Jackson, S.E., Neal, C.R., Chenery, S.P., 1997. A compilation of new and published major and trace element data for NST SRM 610 and NIST SRM 612 glass reference materials. *Geostandard. Newsl.* **21**, 115–144.

Preß, S., Witt, G., Seck, H.A., Eonov, D., Kovalenko, V.I., 1986. Spinel peridotite xenoliths from the Tariat depression, Mongolia. I: major element chemistry and mineralogy of a primitive mantle xenolith suite. *Geochim. Cosmochim. Acta* **50**, 2587–2599.

Qi, Q., Taylor, L.A., Zhou, X., 1995. Petrology and geochemistry of mantle peridotite xenoliths from SE China. *J. Petrol.* **36**, 55–80.

Ravich, M.G., Soloviev, D.S., Fedorov, L.V., 1984. *Geological Structure of MacRobertson Land (East Antarctica)*. Amerind Publishing, New Delhi, p. 230.

Reid, A.M., Dawson, J.B., 1972. Olivine–garnet reaction in peridotites from Tanzania. *Lithos* **5**, 115–124.

Rhodes, J.M., Dawson, J.B., 1975. Major and trace element chemistry of peridotite inclusions from the Lashaine voclano, Tanzania. *Phys. Chem. Earth* **9**, 545–557.

Rudnick, R.L., McDonough, W.F., Orpin, A., 1994. Northern Tanzanian peridotite xenoliths: a comparison with Kaapvaal peridotites and inferences on metasomatic interactions. In: Meyer, H.O.A., Leonardos, O.H. (Eds.), *Kimberlites, Related Rocks and Mantle Xenoliths*. C.P.R.M. Special Publ. 1/A, Brasilia, pp. 336–353.

Sachtleben, T., Seck, H.A., 1981. Chemical control of Al-solubility in orthopyroxene and its implications on pyroxene geothermometry. *Contrib. Mineral. Petrol.* **78**, 157–165.

Schäfer, F.N., Foley, S.F., 2002. The effect of crystal orientation on the wetting behaviour of silicate melts on the surfaces of peridotite minerals. *Contrib. Mineral. Petrol.* **143**, 254–262.

Schiano, P., Bourdon, B., 1999. On the preservation of mantle information in ultramafic nodules: glass inclusions within minerals versus interstitial glasses. *Earth Planet. Sci. Lett.* **169**, 173–188.

Seitz, H.M., Woodland, A.B., 2000. The distribution of lithium in peridotitic and pyroxenitic lithologies—an indicator of magmatic and metasomatic processes. *Chem. Geol.* **166**, 47–64.

Seitz, H.M., Altherr, R., Ludwig, T., 1999. Partitioning of trace elements between orthopyroxene and clinopyroxene in peridotitic and websteritic xenoliths: new empirical geothermometers. *Geochim. Cosmochim. Acta* **63**, 3967–3982.

Seitz, H.M., Brey, G.P., Lahaye, Y., Durali, S., Weyer, S., 2004. Lithium isotopic signatures of peridotite xenoliths and isotopic fractionation at high temperature between olivine and pyroxenes. *Chem. Geol.* **212**, 163–177.

Sheraton, J.W., Tingey, R.J., Black, L.P., Oliver, R.L., 1993. Geology of the Bunger Hills area, Antarctica: implications for Gondwana correlations. *Antarctic Sci.* **5**, 85–102.

Sheraton, J.W., Tindle, A.G., Tingey, R.J., 1996. Geochemistry, origin and tectonic setting of granitic rocks of the Prince Charles Mountains, Antarctica. *AGSO J. Aust. Geol. Geophys.* **16**, 345–370.

Simon, N.S.C., Irvine, G.J., Davies, G.R., Pearson, D.G., Carlson, R.W., 2003. The origin of garnet and clinopyroxene in "depleted" Kaapvaal peridotites. *Lithos* **71**, 289–322.

Skewes, M.A., Stern, C.R., 1979. Petrology and geochemistry of alkali basalts and ultramafic inclusions from the Pali-Aike volcanic field in southern Chile and the origin of the Patagonian lavas. *J. Volcanol. Geotherm. Res.* **6**, 3–25.

Stachel, T., Viljoen, V.S., Grey, G.P., Harris, J.W., 1998. Metasomatic processes in lherzolitic and harzburgitic domains of diamondiferous lithospheric mantle: REE in granets from xenoliths and inclusions in diamond. *Earth Planet. Sci. Lett.* **159**, 1–12.

Stern, C.R., Saul, S., Skewes, M.A., Futa, K., 1989. Garnet peridotite xenoliths from the Pali Aike alkali basalts of southernmost South America. In: Ross, J. et al. (Eds.), *Kimberlites and Related Rocks 2*. Blackwell, Melbourne, pp. 735–744.

Tappe, S., Foley, S.F., Jenner, G.A., Heaman, L.M., Kjarsgaard, B.A., Romer, R.L., Stracke, A., Joyce, N., Hoefs, J., 2006. Genesis of ultrramafic lamprophyres and carbonatites at Aillik Bay, Labrador: a consequence of incipient lithospheric thinning beneath the North Atlantic Craton. *J. Petrol.*, 47. doi:10.1093/petrology/eg1008, March 14th.

Taylor, W.R., Green, D.H., 1987. Measurement of reduced peridotite–C–H–O solidus and implications for redox melting of the mantle. *Nature* **332**, 349–352.

Tingey, R.J., 1991. The regional geology of Archean and Proterozoic rocks in Antarctica. In: Tingey, R.J. (Ed.), *The Geology of Antarctica*. Clarendon Press, Oxford, pp. 1–73.

Vaselli, O., Downes, H., Thirlwall, M., Dobosi, G., Coradossi, N., Seghedi, I., Szakacs, A., Vannucci, R., 1995. Ultramafic xenoliths in Plio-Pleistocene alkali basalts from the Eastern Transylvanian Basin: Depleted mantle enriched by vein metasomatism. *J. Petrol.* **36**, 23–53.

Wells, P.R.A., 1977. Pyroxene thermometry in simple and complex systems. *Contrib. Mineral. Petrol.* **62**, 129–139.

Wilson, D., Aster, R., West, M., Ni, J., Grand, S., Gao, W., Baldrige, W.S., Semken, S., Patel, P., 2005. Lithospheric structure of the Rio Grande rift. *Nature* **433**, 851–855.

Wood, B.J., 1974. Solubility of alumina in orthoyproxene coexisting with garnet. *Contrib. Mineral. Petrol.* **46**, 1–15.

Xu, X., O'Reilly, S.Y., Zhou, X., Griffin, W.L., 1996. A xenolith-derived geotherm and the crust-mantle boundary at Qilin, southeastern China. *Lithos* **38**, 41–62.

Xu, X., O'Reilly, S.Y., Griffin, W.L., Zhou, X., Huang, X., 1998. The nature of the Cenozoic lithosphere at Nushan, eastern China. In: Flower, M.F.J. (Ed.), *Mantle Dynamics and Plate Interactions in East Asia*. American Geophysical Union, Washington, pp. 167–195.

Yaxley, G.M., Kamenetsky, V., Green, D.H., Falloon, T.J., 1997. Glasses in mantle xenoliths from western Victoria, Australia, and their relevance to mantle processes. *Earth Planet. Sci. Lett.* **148**, 433–446.

Zack, T., Foley, S.F., Jenner, G.A., 1997. A consistent partition coefficient set for clinopyroxene, amphibole and garnet from Laser ablation microprobe analysis of garnet pyroxenites from Kakanui, New Zealand. *Neues. Jahrb. Mineral. Abh.* **172**, 23–41.

Zhang, J.P., Zhang, R.Y., Griffin, W.L., Liou, J.G., O'Reilly, S.Y., 2005. Heterogeneous and metasomatized mantle recorded by trace elements inminerals of the Donghai garnet peridotites, Sulu UHP terrane, China. *Chem. Geol.* **221**, 243–259.

Zinngrebe, E., 1998. *Der Inagli Dunit (Sibirien): Ein Beispiel für metasomatische Effekte alkaliner Silikatschmelzen in Peridotiten.* Dr. rer. nat. Dissertation, Göttingen University, Germany, 185pp.

Zinngrebe, E., Foley, S.F., 1995. Metasomatism in mantle xenoliths from Gees, West Eifel, Germany: evidence for the origin of Si–Al rich glasses and the significance of metasomatic Ca-enrichment. *Contrib. Mineral. Petrol.* **122**, 79–96.